

Inverting Laguerre tessellations: Recovering tessellations from the volumes and centroids of their cells using optimal transport

D. P. Bourne*, M. Pearce*, S. M. Roper†

June 4, 2024

Abstract

In this paper we study an inverse problem in convex geometry, inspired by a problem in materials science. Firstly, we consider the question of whether a Laguerre tessellation (a partition by convex polytopes) can be recovered from only the volumes and centroids of its cells. We show that this problem has a unique solution and give a constructive way of computing it using optimal transport theory and convex optimisation. Secondly, we consider the problem of fitting a Laguerre tessellation to synthetic volume and centroid data. Given some target volumes and centroids, we seek a Laguerre tessellation such that the difference between the volumes and centroids of its cells and the target volumes and centroids is minimised. For an appropriate objective function and suitable data, we prove that local minimisers of this problem can be constructed using convex optimisation. We also illustrate our results numerically. There is great interest in the computational materials science community in fitting Laguerre tessellations to electron backscatter diffraction (EBSD) and x-ray diffraction images of polycrystalline materials. As an application of our results we fit a 2D Laguerre tessellation to an EBSD image of steel.

1 Introduction

In this paper we study an inverse problem in computational geometry using tools from optimal transport theory. Laguerre tessellations, also known as power diagrams, are a generalisation of Voronoi tessellations [10, 14, 42]. A Laguerre tessellation is a partition of a set into convex polytopes; see equation (2.1) for the definition. Our goals are the following:

- Goal 1 (inverse problem): Given only the volumes and centroids (barycenters) of the cells in a Laguerre tessellation, can you recover the tessellation?
- Goal 2 (fitting problem): Given a list of target volumes and centroids, can you find a Laguerre tessellation such that the volumes and centroids of the Laguerre cells give the ‘best fit’ of the target volumes and centroids?

These goals are stated precisely in Section 3.

*Maxwell Institute for Mathematical Sciences and Department of Mathematics, Heriot-Watt University, Edinburgh, UK

†School of Mathematics and Statistics, University of Glasgow, Glasgow, UK

Motivation. There are numerous applications of Laguerre tessellations including cell biology [13, 22], domain decomposition [52], fluid mechanics [25], foam modelling [18, 34], image interpolation [32], mesh generation [33], optics [40], optimal location problems [17], sampling [37] and the proof of the Nandakumar and Ramana Rao conjecture [12].

Our main motivation comes from materials science, where Laguerre tessellations are often used to represent the microstructure of polycrystalline materials, such as metals [24, 30, 51, 35, 49, 21, 15, 29, 16]. They are used for both synthetic microstructure generation and for imaging. For these applications it is important to have efficient algorithms for generating Laguerre tessellations with prescribed geometrical and statistical properties, such as the volumes of the cells, their shape and their spatial distribution. In this paper we focus on controlling the volumes and the centroids of the cells, the latter of which gives some control over the locations of the cells.

Previous work. The phrase *inverting Laguerre tessellations* comes from the paper [23], where the authors studied the problem of recovering the *generators* of a 2D normal Laguerre tessellation from the tessellation itself (from the edges and vertices). The generators are not uniquely determined by the tessellation, but they can be recovered uniquely once you have fixed the generator (seed and weight) of one interior cell and one coordinate of the seed of an adjacent cell; see [23, Theorem 3.1]. This non-uniqueness is also discussed in Lemma 2.1 below. In [23] the authors solved the same problem numerically using the cross-entropy method.

The inverse problem that we study in Goal 1 is a little different; we seek to recover the tessellation given the volumes and centroids of the cells. In the process we recover one set of generators from the infinite family of possible generators.

Another inverse problem is to determine whether a partition by convex polytopes is a Laguerre tessellation. This is addressed in [8] and [31, Theorem 3.2].

Several variations of Goal 2 have been studied in the materials science literature, motivated by the application of fitting Laguerre diagrams and anisotropic Laguerre diagrams to images of metals, such as electron backscatter diffraction (EBSD) images or x-ray diffraction (XRD) images [4, 49, 48, 45, 44, 43, 6]. In Section 5.3 we fit a Laguerre tessellation to a 2D EBSD image of steel. An EBSD image can be thought of as an assignment map, which associates each pixel in the image to a ‘cell’ (grain) in the metal.

The main difference between our work and these previous works is the choice of objective function. In our work the objective function measures the mismatch between the actual centroids of the Laguerre cells and the target centroids, which are the centroids of the cells in the EBSD image. The areas of the cells are fitted ‘exactly’, up to any desired tolerance. In most of the previous works listed above, the objective function measures the number of misassigned pixels in the image (the pixels assigned to the wrong Laguerre cells). The objective function in [44] is closest in spirit to ours, where the authors minimise a weighted sum of the volume and centroid error. Moreover, most of the works above use the full EBSD/XRD image (assignment map), whereas in our work and [44] only the areas and centroids of the cells in the image are used, and the rest of the data is discarded. The common feature of our work is the use of optimisation algorithms.

An entirely different approach is given in [50], where they propose an optimisation-free method for fitting an (anisotropic) Laguerre tessellation to an EBSD image. Their heuristic gives good results for little computational effort. In this paper we give a partial explanation

for this, as a by-product of our solution of Goal 2.

Contributions. Here is a summary of our main contributions:

- Goal 1: We prove that a Laguerre tessellation is uniquely determined by the volumes and centroids of its cells (Theorem 4.5) and that it can be recovered by solving an unconstrained convex optimisation problem (Theorem 4.6). In the language of machine learning, one would say that a Laguerre tessellation can be learnt from the volumes and centroids of its cells. We generalise these results to anisotropic Laguerre tessellations (Section 6).
- Goal 2: We prove that, under suitable assumptions on the target volumes and centroids, fitting a Laguerre tessellation to volume and centroid data is also essentially a convex optimisation problem, in the sense that local minimisers of the least-squares fitting error can be found by solving a constrained convex optimisation problem (Theorem 4.11). The assumptions on the target volumes and centroids, however, are implicit and potentially quite restrictive, as illustrated numerically in Section 5.2
- Justification of a popular heuristic in the literature: A popular heuristic for approximately solving Goal 2 is to take the seeds of the Laguerre diagram to be the target centroids [50]. In Remark 4.13 we give a partial justification for why this heuristic works so well.
- Application in computational materials science: As an application of Goal 2, we fit a Laguerre tessellation to an EBSD image of a single-phase steel, provided to us by Tata Steel Europe (Section 5.3).

Methods. Our main theoretical tool is *optimal transport theory* [47], in particular *semi-discrete optimal transport* [38, Section 4], which has strong links to computational geometry. In Section 2.2 we recall how a Laguerre tessellation with cells of prescribed volumes can be computed efficiently by solving a semi-discrete optimal transport problem; see Theorem 2.2. The simulations in Section 5 rely on a modern numerical method for optimal transport, the damped Newton method [28], and a fast Python implementation using the library *pysdot* [3].

Outline of the paper. Section 2 includes the necessary background material on Laguerre tessellations and semi-discrete optimal transport theory. The goals of the paper are stated in Section 3. Section 4 contains our main theoretical results. Section 4.1 introduces the concave function H , which is important throughout the rest of the paper. Goal 1 is addressed in Section 4.2 and Goal 2 is addressed in Sections 4.3 and 4.4. Section 5 contains our numerical results. In particular, we solve Goal 1 numerically in Section 5.1 and Goal 2 numerically in Section 5.2. In Section 5.3 we give an application of Goal 2 in computational materials science (fitting a Laguerre tessellation to an EBSD image). Finally, in Section 6 we show how our results for Goal 1 can be generalised to anisotropic Laguerre diagrams.

2 Background material

2.1 Laguerre tessellations

Let $d \in \mathbb{N}$, $d \geq 2$. Throughout this paper we take $\Omega \subset \mathbb{R}^d$ to be a non-empty, convex, bounded set that is equal to the closure of its interior. In the numerical experiments in Section 5 we take $d = 2$ and Ω to be a rectangular domain. A Laguerre tessellation of Ω is a collection of sets that partitions Ω into convex regions (convex polytopes if Ω is a polytope). The partition is parameterised by a set of seeds and a corresponding set of weights. Define the set of distinct seeds by

$$\mathbb{D}_n = \{\mathbf{X} = (x_1, \dots, x_n) \in (\mathbb{R}^d)^n : x_i \neq x_j \forall i, j \in \{1, \dots, n\}, i \neq j\}.$$

Given $\mathbf{X} \in \mathbb{D}_n$ and a set of weights $\mathbf{w} = (w_1, \dots, w_n)$, $w_i \in \mathbb{R}$, the i^{th} Laguerre cell generated by (\mathbf{X}, \mathbf{w}) is defined by

$$\text{Lag}_i(\mathbf{X}, \mathbf{w}) = \{x \in \Omega : |x - x_i|^2 - w_i \leq |x - x_j|^2 - w_j \forall j \in \{1, \dots, n\}\}, \quad (2.1)$$

where $|\cdot|$ denotes the standard Euclidean norm. The Laguerre tessellation generated by (\mathbf{X}, \mathbf{w}) is the collection of cells $\{\text{Lag}_i(\mathbf{X}, \mathbf{w})\}_{i=1}^n$. To see that the Laguerre cells are convex, note that they can be written as an intersection of convex sets:

$$\text{Lag}_i(\mathbf{X}, \mathbf{w}) = \Omega \cap \bigcap_{j \neq i} H_{ij}(\mathbf{X}, \mathbf{w}), \quad (2.2)$$

where H_{ij} is the half-space

$$H_{ij}(\mathbf{X}, \mathbf{w}) = \{x \in \mathbb{R}^d : |x - x_i|^2 - w_i \leq |x - x_j|^2 - w_j\}.$$

Furthermore, all the cells are convex polygons (if $d = 2$) or convex polyhedra (if $d = 3$), except possibly for the cells that intersect the boundary of Ω .

Definition (2.1) can be extended to the case where the seeds are non-distinct, however the corresponding cells do not necessarily form a tessellation. If two seeds coincide their cells are either equal or one is the empty-set, depending on the values of the corresponding weights.

The parameterisation of the tessellation is non-unique; observe that if we add a constant to all the weights ($w_i \mapsto w_i + c$ for all i), then the inequalities in (2.1) are still satisfied and the cells remain unchanged. Moreover, the following lemma asserts that we can uniformly translate and dilate the seeds without changing the Laguerre tessellation, provided that the weights are adjusted appropriately.

Lemma 2.1 (See [39], Proposition 6). *Let $\mathbf{X}_1 = (x_1^1, \dots, x_n^1) \in \mathbb{D}_n$ and $\mathbf{w}_1 = (w_1^1, \dots, w_n^1) \in \mathbb{R}^n$ be the generators of a Laguerre tessellation. Given a dilation factor $\lambda > 0$ and translation $t \in \mathbb{R}^d$, define $\mathbf{X}_2 = (x_1^2, \dots, x_n^2)$ by $x_i^2 = \lambda x_i^1 + t$. Let*

$$w_i^2 = \lambda w_i^1 + 2\lambda t \cdot x_i^1 + \lambda(\lambda - 1)|x_i^1|^2, \quad i \in \{1, \dots, n\}. \quad (2.3)$$

Then $\text{Lag}_i(\mathbf{X}_1, \mathbf{w}_1) = \text{Lag}_i(\mathbf{X}_2, \mathbf{w}_2)$ for all $i \in \{1, \dots, n\}$.

Given a (Lebesgue-measurable) set $A \subseteq \mathbb{R}^d$, we define $\text{vol}(A)$ to be its d -dimensional volume (area if $d = 2$, volume if $d = 3$) and $\sigma(A)$ to be its centroid:

$$\text{vol}(A) = \int_A 1 \, dx, \quad \sigma(A) = \frac{1}{\text{vol}(A)} \int_A x \, dx.$$

The latter is only defined for A such that $\text{vol}(A)$ is non-zero. Given $(\mathbf{X}, \mathbf{w}) \in \mathbb{D}_n \times \mathbb{R}^n$, we denote the volume and centroid of the Laguerre cell $\text{Lag}_i(\mathbf{X}, \mathbf{w})$ by

$$m_i(\mathbf{X}, \mathbf{w}) = \text{vol}(\text{Lag}_i(\mathbf{X}, \mathbf{w})), \quad \xi_i(\mathbf{X}, \mathbf{w}) = \sigma(\text{Lag}_i(\mathbf{X}, \mathbf{w})). \quad (2.4)$$

Since the Laguerre cells are disjoint (up to sets of measure zero), we have

$$\text{vol}(\Omega) = \int_{\Omega} 1 \, dx = \sum_{i=1}^n \int_{\text{Lag}_i(\mathbf{X}, \mathbf{w})} 1 \, dx = \sum_{i=1}^n m_i(\mathbf{X}, \mathbf{w}), \quad (2.5)$$

$$\text{vol}(\Omega) \cdot \sigma(\Omega) = \int_{\Omega} x \, dx = \sum_{i=1}^n \int_{\text{Lag}_i(\mathbf{X}, \mathbf{w})} x \, dx = \sum_{i=1}^n m_i(\mathbf{X}, \mathbf{w}) \xi_i(\mathbf{X}, \mathbf{w}). \quad (2.6)$$

There is a one-to-one correspondence between Laguerre tessellations and solutions of semi-discrete optimal transport problems, which is useful for generating Laguerre tessellations with cells of prescribed volumes, as described in the next section.

2.2 Link to semi-discrete optimal transport

Define $\mathbb{R}_+ = (0, \infty)$ and

$$\mathbb{V}_n = \left\{ \mathbf{v} = (v_1, \dots, v_n) \in \mathbb{R}_+^n : \sum_{i=1}^n v_i = \text{vol}(\Omega) \right\}.$$

Given $\mathbf{X} = (x_1, \dots, x_n) \in (\mathbb{R}^d)^n$ and $v \in \mathbb{V}_n$, we define the measure $\nu(\mathbf{X}, \mathbf{v}) \in \mathcal{M}_+(\mathbb{R}^d)$ by

$$\nu(\mathbf{X}, \mathbf{v}) = \sum_{i=1}^n v_i \delta_{x_i},$$

where δ_{x_i} denotes the Dirac measure supported at $\{x_i\}$. This is well defined even if the seeds x_i are not distinct.

Let \mathcal{L}_{Ω}^d be the d -dimensional Lebesgue measure restricted to Ω . Any map $T : \Omega \rightarrow \{x_1, \dots, x_n\}$ satisfying $\text{vol}(T^{-1}(\{x_i\})) = v_i$ for all i is called an *admissible transport map*. We denote the set of admissible transport maps by $\mathcal{A}(\mathbf{X}, \mathbf{v})$:

$$\mathcal{A}(\mathbf{X}, \mathbf{v}) = \{T : \Omega \rightarrow \{x_1, \dots, x_n\} : \text{vol}(T^{-1}(\{x_i\})) = v_i \, \forall \, i \in \{1, \dots, n\}\}. \quad (2.7)$$

For any $T \in \mathcal{A}(\mathbf{X}, \mathbf{v})$ we define the *transport cost* $M(T)$ by

$$M(T) := \int_{\Omega} |x - T(x)|^2 \, dx = \sum_{i=1}^n \int_{T^{-1}(\{x_i\})} |x - x_i|^2 \, dx.$$

The *optimal cost* of transporting \mathcal{L}_{Ω}^d to $\nu(\mathbf{X}, \mathbf{v})$ is

$$\mathcal{T}(\mathbf{X}, \mathbf{v}) = \inf_{T \in \mathcal{A}(\mathbf{X}, \mathbf{v})} M(T). \quad (2.8)$$

Any minimiser T^* in (2.8) is called an *optimal transport map*, and

$$W_2(\mathcal{L}_{\Omega}^d, \nu(\mathbf{X}, \mathbf{v})) := \mathcal{T}(\mathbf{X}, \mathbf{v})^{1/2} \quad (2.9)$$

is the *Wasserstein distance* between the measures \mathcal{L}_Ω^d and $\nu(\mathbf{X}, \mathbf{w})$. See for example [47]

It is well-known, see for instance [38], that there exists an optimal transport map T^* , it is unique (almost everywhere), it is the gradient of a convex function, and it has the following form: There exists $\mathbf{w} = (w_1, \dots, w_n) \in \mathbb{R}^n$ such that

$$T^*(x) = x_i \quad \text{if } x \in \text{int Lag}_i(\mathbf{X}, \mathbf{w}), \quad (2.10)$$

where int denotes the interior. This defines T^* uniquely almost everywhere because the boundaries of the cells form a set of measure zero. In particular, $(T^*)^{-1}(\{x_i\})$ is the Laguerre cell $\text{Lag}_i(\mathbf{X}, \mathbf{w})$ (up to a set of measure zero) with $\text{vol}(\text{Lag}_i(\mathbf{X}, \mathbf{w})) = v_i$ for all i .

The following theorem gives us a method to find the weights \mathbf{w} and consequently the optimal map (2.10). It goes back at least as far as [9] and is well-known in the optimal transport community.

Theorem 2.2 (See [38], Theorem 40 & Proposition 37). *Given $\mathbf{X} \in \mathbb{D}_n$ and $\mathbf{v} \in \mathbb{V}_n$, define the dual function $\mathcal{K} : \mathbb{R}^n \rightarrow \mathbb{R}$ by*

$$\mathcal{K}(\mathbf{w}) = \int_{\Omega} \min_i (|x - x_i|^2 - w_i) dx + \sum_{i=1}^n w_i v_i = \sum_{i=1}^n \int_{\text{Lag}_i(\mathbf{X}, \mathbf{w})} (|x - x_i|^2 - w_i) dx + \sum_{i=1}^n w_i v_i.$$

Then $\mathcal{K} \in C^1(\mathbb{R}^n)$, it is concave, and its gradient is given by

$$\frac{\partial \mathcal{K}}{\partial w_i}(\mathbf{w}) = v_i - m_i(\mathbf{X}, \mathbf{w}) \quad \forall i \in \{1, \dots, n\}.$$

Moreover

$$\min_{T \in \mathcal{A}(\mathbf{X}, \mathbf{v})} \mathcal{M}(T) = \max_{\mathbf{w} \in \mathbb{R}^n} \mathcal{K}(\mathbf{w}).$$

In particular, the maximum of \mathcal{K} is achieved. Let $w^* \in \mathbb{R}^n$ be a maximiser of \mathcal{K} . Then $T_{\mathbf{w}^*} : \Omega \rightarrow \{x_1, \dots, x_n\}$ defined almost everywhere by

$$T_{\mathbf{w}^*}(x) := x_i \quad \text{if } x \in \text{int Lag}_i(\mathbf{X}, \mathbf{w}^*)$$

is the optimal transport map for (2.8). Furthermore,

$$\text{vol}(\text{Lag}_i(\mathbf{X}, \mathbf{w}^*)) = v_i \quad \forall i \in \{1, \dots, n\}.$$

In summary, \mathbf{w}^* maximises \mathcal{K} if and only if the Laguerre cells $\text{Lag}_i(\mathbf{X}, \mathbf{w}^*)$ have the desired volumes v_i . The optimal weight vector, \mathbf{w}^* , is not unique since we can add a constant vector to \mathbf{w}^* and the cells are unchanged. However, if we fix a value for one of the weights we have uniqueness. Usually we chose $w_n = 0$ since this is easy to implement computationally. From now on, we let $\mathbf{w}^*(\mathbf{X}; \mathbf{v})$ denote the unique optimal weight vector with $w_n^*(\mathbf{X}; \mathbf{v}) = 0$. By definition (see (2.4)),

$$m_i(\mathbf{X}, \mathbf{w}^*(\mathbf{X}; \mathbf{v})) = v_i \quad \forall i \in \{1, \dots, n\}.$$

We define $L_i(\mathbf{X}; \mathbf{v})$ to be the i^{th} Laguerre cell in the tessellation with seeds \mathbf{X} and cell volumes \mathbf{v} , and $c_i(\mathbf{X}; \mathbf{v})$ to be its centroid:

$$L_i(\mathbf{X}; \mathbf{v}) = \text{Lag}_i(\mathbf{X}, \mathbf{w}^*(\mathbf{X}; \mathbf{v})), \quad (2.11)$$

$$c_i(\mathbf{X}; \mathbf{v}) = \xi_i(\mathbf{X}; \mathbf{w}^*(\mathbf{X}; \mathbf{v})). \quad (2.12)$$

In this notation, by Theorem 2.2,

$$W_2^2(\mathcal{L}_\Omega^d, \nu(\mathbf{X}, \mathbf{v})) = \sum_{i=1}^n \int_{L_i(\mathbf{X}; \mathbf{v})} |x - x_i|^2 dx. \quad (2.13)$$

The state-of-the-art method for maximising \mathcal{K} is the damped-Newton method, which can be found in [28] and [38, Algorithm 4]. This is implemented for example in the software libraries `geogram` [1], `MATLAB-SDOT` [2] and `pysdot` [3]. We use `pysdot` for the simulations in Section 5.

3 Statement of the problems

Our first goal is to invert a Laguerre tessellation in the following sense. We wish to recover a Laguerre tessellation only from the knowledge of the volumes and centroids of its cells. To be precise, we consider the following inverse problem:

Goal 1 (Inverting a Laguerre tessellation). *Let $\mathbf{X} \in \mathbb{D}_n$ and $\mathbf{w} \in \mathbb{R}^n$. For $i \in \{1, \dots, n\}$, define $v_i = m_i(\mathbf{X}, \mathbf{w})$ and $b_i = \xi_i(\mathbf{X}, \mathbf{w})$ to be the volume and centroid of the Laguerre cell $\text{Lag}_i(\mathbf{X}, \mathbf{w})$. The goal is to recover the Laguerre cells $\text{Lag}_i(\mathbf{X}, \mathbf{w})$ given only $\mathbf{v} = (v_1, \dots, v_n)$ and $\mathbf{B} = (b_1, \dots, b_n)$.*

We prove that this problem has a unique solution in Theorem 4.5, in the sense that the Laguerre cells $\text{Lag}_i(\mathbf{X}, \mathbf{w})$ are unique. The generators (\mathbf{X}, \mathbf{w}) are not unique because (by Lemma 2.1) the seeds can be uniformly translated and dilated and a constant can be added to the weights without changing the Laguerre cells. We also give a constructive method for recovering $\text{Lag}_i(\mathbf{X}, \mathbf{w})$ from (\mathbf{v}, \mathbf{B}) by solving an unconstrained convex optimisation problem; see Theorem 4.6. This is illustrated numerically in Section 5.1. We consider the generalisation of inverting *anisotropic* Laguerre tessellations in Section 6.

Our second goal is, given some target volumes and centroids (not coming from a Laguerre tessellation), find a Laguerre tessellation that best fits this data. To state the problem precisely we need some more notation. Let \mathcal{D}_n denote the set of target volumes and centroids (or barycentres):

$$\mathcal{D}_n = \left\{ (\mathbf{v}, \mathbf{B}) = ((v_1, \dots, v_n), (b_1, \dots, b_n)) \in \mathbb{V}_n \times \Omega^n : \right. \\ \left. \sum_{i=1}^n v_i = \text{vol}(\Omega), \quad \sum_{i=1}^n v_i b_i = \text{vol}(\Omega) \sigma(\Omega) \right\}.$$

The constraints on (\mathbf{v}, \mathbf{B}) stem from (2.5) and (2.6). They are necessary for there to exist a Laguerre tessellation with cells with volumes v_i and centroids b_i . We refer to the elements $(\mathbf{v}, \mathbf{B}) \in \mathcal{D}_n$ as *compatible data* for the domain Ω .

Given a domain Ω and a compatible set of target volumes and centroids $(\mathbf{v}, \mathbf{B}) \in \mathcal{D}_n$, the goal is to find a Laguerre tessellation with cells of volume v_i and minimal centroid error. To be precise, we consider the following data-fitting problem:

Goal 2 (Fitting a Laguerre tessellation). *Let $(\mathbf{v}, \mathbf{B}) \in \mathcal{D}_n$. The goal is to solve the nonlinear least squares problem*

$$\inf_{\mathbf{X} \in \mathbb{D}_n} f(\mathbf{X}; (\mathbf{v}, \mathbf{B})) \quad (\text{NLS})$$

where $f : \mathbb{D}_n \rightarrow \mathbb{R}$ is defined by

$$f(\mathbf{X}; (\mathbf{v}, \mathbf{B})) = \sum_{i=1}^n v_i^2 |c_i(\mathbf{X}; \mathbf{v}) - b_i|^2. \quad (3.1)$$

Note that the objective function can be expressed in terms of first moments of the Laguerre cells:

$$f(\mathbf{X}; (\mathbf{v}, \mathbf{B})) = \sum_{i=1}^n \left| \int_{L_i(\mathbf{X}; \mathbf{v})} x \, dx - v_i b_i \right|^2.$$

We choose to fit the zeroth moments (the volumes) exactly and to approximately fit the first moments. In other words, we choose the weights \mathbf{v} so that the Laguerre cells have the desired volumes, and we choose the seeds \mathbf{X} to minimise the centroid error. Alternatively, instead of fitting the volumes exactly, one could minimise a weighted sum of the volume and centroid error over (\mathbf{X}, \mathbf{w}) , as in [44]. One advantage of our approach is that, for some data (\mathbf{v}, \mathbf{B}) , (NLS) turns out to be essentially equivalent to a convex optimisation problem, as we will see in Section 4.4. One disadvantage of our approach is that the set \mathbb{D}_n is not compact and so the optimisation problem (NLS) may not have a solution; the infimum may not be attained. For some data (\mathbf{v}, \mathbf{B}) , infimising sequences (\mathbf{X}_k) in \mathbb{D}_n converge to a point in $\mathbb{R}^{nd} \setminus \mathbb{D}_n$ with non-distinct seeds. We illustrate this point numerically in Section 5.2. We give a practical example of fitting a Laguerre tessellation to data coming from an EBSD image of steel in Section 5.3.

We also give necessary (but not sufficient) conditions on the data (\mathbf{v}, \mathbf{B}) for there to exist $\mathbf{X} \in \mathbb{D}_n$ such that $f(\mathbf{X}; (\mathbf{v}, \mathbf{B})) = 0$, that is, for there to exist a Laguerre diagram with cells of volumes \mathbf{v} and centroids \mathbf{B} ; see Section 4.3.

4 Main results

4.1 The helper function H

The following function will be very important in our analysis. Given $(\mathbf{v}, \mathbf{B}) \in \mathcal{D}_n$, define $H : \mathbb{R}^{nd} \rightarrow \mathbb{R}$ by

$$H(\mathbf{X}) = H(\mathbf{X}; (\mathbf{v}, \mathbf{B})) = F(\mathbf{X}; \mathbf{v}) - \frac{1}{2} \sum_{i=1}^n v_i |x_i|^2 + \sum_{i=1}^n v_i x_i \cdot b_i - \frac{1}{2} \int_{\Omega} |x|^2 \, dx, \quad (4.1)$$

where $F : \mathbb{R}^{nd} \rightarrow \mathbb{R}$ is defined by

$$F(\mathbf{X}) = F(\mathbf{X}; \mathbf{v}) = \frac{1}{2} W_2^2(\mathcal{L}_{\Omega}^d, \nu(\mathbf{X}, \mathbf{v})), \quad (4.2)$$

and W_2 was defined in (2.9). First we recall a fact about F .

Theorem 4.1 (Derivative of W_2^2 ; cf. [37], Proposition 1). *The function $F : \mathbb{R}^{nd} \rightarrow \mathbb{R}$ is semi-concave in the sense that the function $\mathbf{X} \mapsto F(\mathbf{X}) - \frac{1}{2} \sum_{i=1}^n v_i |x_i|^2$ is concave. Moreover, F is continuously differentiable on the set of distinct seeds, $F \in C^1(\mathbb{D}_n)$, and*

$$\frac{\partial F}{\partial x_i}(\mathbf{X}) = v_i(x_i - c_i(\mathbf{X}; \mathbf{v})) \quad \forall i \in \{1, \dots, n\}.$$

The previous result is crucial in proving the following.

Theorem 4.2 (Properties of H). *Let $(\mathbf{v}, \mathbf{B}) \in \mathcal{D}_n$ and $H : \mathbb{R}^{nd} \rightarrow \mathbb{R}$ be the function defined in equation (4.1).*

(i) *If $\mathbf{X} \in \mathbb{D}_n$, then*

$$H(\mathbf{X}) = \sum_{i=1}^n v_i (b_i - c_i(\mathbf{X}; \mathbf{v})) \cdot x_i. \quad (4.3)$$

In particular, if $\mathbf{X} \in \mathbb{D}_n$ generates a Laguerre tessellation with cells of volume v_i and centroids b_i , then $H(\mathbf{X}) = 0$.

(ii) *Let $x_1 \in \mathbb{R}^d$ and $\mathbf{X} = (x_1, \dots, x_1) \in \mathbb{R}^{nd}$. Then $H(\mathbf{X}) = 0$.*

(iii) *H is concave.*

(iv) *H is continuously differentiable on the set of distinct seeds, $H \in C^1(\mathbb{D}_n)$, and for all $\mathbf{X} \in \mathbb{D}_n$ the gradient of H is given by*

$$\frac{\partial H}{\partial x_i}(\mathbf{X}) = v_i (b_i - c_i(\mathbf{X}; \mathbf{v})) \quad \forall i \in \{1, \dots, n\}.$$

In particular, $\nabla H(\mathbf{X}) = 0$ if and only if \mathbf{X} generates a Laguerre tessellation with cells of volume v_i and centroids b_i . Moreover, the objective function f defined in (3.1) is related to H by

$$f(\mathbf{X}) = |\nabla H(\mathbf{X})|^2. \quad (4.4)$$

(v) *Let $\mathbf{X} \in \mathbb{R}^{nd}$, $\lambda \geq 0$, $t \in \mathbb{R}^d$, $\mathbf{T} = (t, \dots, t) \in \mathbb{R}^{nd}$. Then*

$$H(\lambda \mathbf{X} + \mathbf{T}) = \lambda H(\mathbf{X}).$$

In particular, H is 1-positively homogeneous and, for all $\mathbf{X} \in \mathbb{D}_n$,

$$\nabla H(\lambda \mathbf{X} + \mathbf{T}) = \nabla H(\mathbf{X}). \quad (4.5)$$

Moreover, for all $\lambda \in \mathbb{R}$ and $\mathbf{X} \in \mathbb{R}^{nd}$,

$$H(\lambda \mathbf{X}) \leq \lambda H(\mathbf{X})$$

with equality if $\lambda \geq 0$.

(vi) *H is superlinear, that is, for all $\mathbf{X}, \mathbf{Y} \in \mathbb{R}^{nd}$,*

$$H(\mathbf{X} + \mathbf{Y}) \geq H(\mathbf{X}) + H(\mathbf{Y}).$$

(vii) *If there exists $\mathbf{X}^* \in \mathbb{D}_n$ such that $c_i(\mathbf{X}^*; \mathbf{v}) = b_i$ for all $i \in \{1, \dots, n\}$, then*

$$\max_{\mathbf{X} \in \mathbb{R}^{nd}} H(\mathbf{X}) = H(\mathbf{X}^*) = 0.$$

If not, then either

$$\sup_{\mathbf{X} \in \mathbb{R}^{nd}} H(\mathbf{X}) = +\infty$$

or

$$\max_{\mathbf{X} \in \mathbb{R}^{nd}} H(\mathbf{X}) = 0 = H((x_1, \dots, x_1))$$

for any $x_1 \in \mathbb{R}^d$.

(viii) Let $K \subset \mathbb{R}^{nd}$ be compact. If there does not exist a Laguerre tessellation with cells of volume v_i and centroids b_i , then either the maximum of H over K is achieved on ∂K or it is achieved on the set of non-distinct seeds $K \setminus \mathbb{D}_n$.

Proof.

(i) The first claim can be proved via a simple algebraic manipulation as follows. By definition of H and equation (2.13),

$$\begin{aligned} H(\mathbf{X}) &= \frac{1}{2} \sum_{i=1}^n \int_{L_i(\mathbf{X}; \mathbf{v})} |x - x_i|^2 dx - \frac{1}{2} \sum_{i=1}^n v_i |x_i|^2 + \sum_{i=1}^n v_i x_i \cdot b_i - \frac{1}{2} \int_{\Omega} |x|^2 dx \\ &= \sum_{i=1}^n v_i (b_i - c_i(\mathbf{X}; \mathbf{v})) \cdot x_i. \end{aligned}$$

(ii) Observe that if $\mathbf{X} = (x_1, \dots, x_1)$ for $x_1 \in \mathbb{R}^d$, then

$$\begin{aligned} H(\mathbf{X}) &= \frac{1}{2} \int_{\Omega} |x - x_1|^2 dx - \frac{1}{2} \sum_{i=1}^n v_i |x_1|^2 + \sum_{i=1}^n v_i x_1 \cdot b_i - \frac{1}{2} \int_{\Omega} |x|^2 dx \\ &= x_1 \cdot \left(-\text{vol}(\Omega)\sigma(\Omega) + \sum_{i=1}^n v_i b_i \right) \\ &= 0, \end{aligned}$$

where the last two equalities follow from the assumption that $(\mathbf{v}, \mathbf{B}) \in \mathcal{D}_n$. Alternatively, one can deduce that $H(\mathbf{X}) = 0$ by letting $\lambda \rightarrow 0^+$ in part (v).

(iii) The proof follows the same argument found in [36, Propostion 21]. It suffices to show that the map

$$\mathbf{X} \mapsto 2F(\mathbf{X}; \mathbf{v}) - \sum_{i=1}^n v_i |x_i|^2 = \min_{T \in \mathcal{A}(\mathbf{X}, \mathbf{v})} \int_{\Omega} |x - T(x)|^2 dx - \sum_{i=1}^n v_i |x_i|^2$$

is concave since the remaining terms of H are affine in \mathbf{X} . Let $\mathcal{P}(\Omega, \mathbf{v})$ denote the set of partitions of Ω with cells of volume \mathbf{v} :

$$\mathcal{P}(\Omega, \mathbf{v}) = \left\{ (P_i)_{i=1}^n : P_i \in \mathcal{B}(\Omega), \text{vol}(P_i) = v_i, \bigcup_{i=1}^n P_i = \Omega, \text{vol}(P_i \cap P_j) = 0 \text{ if } i \neq j \right\},$$

where $\mathcal{B}(\Omega)$ is the Borel sigma-algebra of Ω . Then equivalently,

$$2F(\mathbf{X}; \mathbf{v}) - \sum_{i=1}^n v_i |x_i|^2 = \inf_{(P_i)_{i=1}^n \in \mathcal{P}(\Omega, \mathbf{v})} \sum_{i=1}^n \int_{P_i} |x - x_i|^2 dx - \sum_{i=1}^n v_i |x_i|^2 \quad (4.6)$$

since any $(P_i)_{i=1}^n \in \mathcal{P}(\Omega, \mathbf{v})$ induces an admissible map given by $T(x) = x_i$ if $x \in P_i$ and conversely any admissible map gives rise to a partition. Simplifying (4.6) we find that

$$2F(\mathbf{X}, \mathbf{v}) - \sum_{i=1}^n v_i |x_i|^2 = \inf_{(P)_{i=1}^n \in \mathcal{P}(\mathbf{X}, \mathbf{v})} \sum_{i=1}^n \int_{P_i} (|x|^2 - 2x \cdot x_i) dx,$$

which is the pointwise infimum of a family of affine functions of \mathbf{X} , and hence is concave.

(iv) Theorem 4.1 implies that H is continuously differentiable in \mathbb{D}_n and immediately gives the expression for its gradient.

(v) Let \mathbf{X}, λ, t and \mathbf{T} be defined as in the statement of the theorem. Then, for all $i \in \{1, \dots, n\}$, $L_i(\mathbf{X}; \mathbf{v}) = L_i(\lambda\mathbf{X} + \mathbf{T}; \mathbf{v})$ by Lemma 2.1 and the uniqueness of optimal transport maps. Consequently, if $X \in \mathbb{D}_n$ and $\lambda > 0$, then

$$H(\lambda\mathbf{X} + \mathbf{T}) \stackrel{(4.3)}{=} \sum_{i=1}^n v_i(b_i - c_i(\lambda\mathbf{X} + \mathbf{T}; \mathbf{v})) \cdot (\lambda x_i + t) = \sum_{i=1}^n v_i(b_i - c_i(\mathbf{X}; \mathbf{v})) \cdot (\lambda x_i + t).$$

Recall that $(\mathbf{v}, \mathbf{B}) \in \mathbb{D}_n$ implies that $\sum_{i=1}^n v_i b_i = \text{vol}(\Omega)\sigma(\Omega) = \sum_{i=1}^n v_i c_i(\mathbf{X}; \mathbf{v})$. Therefore $t \cdot \sum_{i=1}^n v_i (b_i - c_i(\mathbf{X}; \mathbf{v})) = 0$ and so

$$H(\lambda\mathbf{X} + \mathbf{T}) = \sum_{i=1}^n v_i (b_i - c_i(\mathbf{X}; \mathbf{v})) \cdot \lambda x_i = \lambda \sum_{i=1}^n v_i (b_i - c_i(\mathbf{X}; \mathbf{v})) \cdot x_i \stackrel{(4.3)}{=} \lambda H(\mathbf{X}),$$

which establishes the result for $\mathbf{X} \in \mathbb{D}_n$. The general result for $\mathbf{X} \in \mathbb{R}^{nd}$ and $\lambda = 0$ can be established from the continuity of H . The expression $\nabla H(\mathbf{X}) = \nabla H(\lambda\mathbf{X} + \mathbf{T})$ follows immediately from the chain rule. Finally, to prove that $H(\lambda\mathbf{X}) \leq \lambda H(\mathbf{X})$ for all $\lambda \in \mathbb{R}$, it suffices to show that $H(-\mathbf{X}) \leq -H(\mathbf{X})$ since then, for all $\lambda < 0$,

$$H(\lambda\mathbf{X}) = H((-\lambda)(-\mathbf{X})) = -\lambda H(-\mathbf{X}) \leq \lambda H(\mathbf{X}).$$

Since $H(\mathbf{0}) = 0$ (by (ii)) and H is concave we have,

$$0 = H(\mathbf{0}) = H\left(\frac{1}{2}\mathbf{X} + \frac{1}{2}(-\mathbf{X})\right) \geq \frac{1}{2}H(\mathbf{X}) + \frac{1}{2}H(-\mathbf{X}) \iff H(-\mathbf{X}) \leq -H(\mathbf{X}),$$

as required.

(vi) Let $\mathbf{X}, \mathbf{Y} \in \mathbb{R}^{nd}$. Then by positive homogeneity and concavity,

$$\frac{1}{2}H(\mathbf{X} + \mathbf{Y}) = H\left(\frac{1}{2}\mathbf{X} + \frac{1}{2}\mathbf{Y}\right) \geq \frac{1}{2}(H(\mathbf{X}) + H(\mathbf{Y})).$$

Multiplying both sides by 2 gives the desired result.

(vii) If there exists $\mathbf{X}^* \in \mathbb{D}_n$ such that $c_i(\mathbf{X}^*; \mathbf{v}) = b_i$, then $\nabla H(\mathbf{X}^*) = 0$ by (iv). Since H is concave, it follows that X^* is a global maximiser of H . Furthermore, $H(\mathbf{X}^*) = 0$ by (i). If there does not exist such an $\mathbf{X}^* \in \mathbb{D}_n$, then there are two cases. Either there exists $\mathbf{X} \in \mathbb{R}^{nd}$ such that $H(\mathbf{X}) > 0$, in which case $\lim_{\lambda \rightarrow \infty} H(\lambda\mathbf{X}) = +\infty$. Or, if $H(\mathbf{X}) \leq 0$ for all $\mathbf{X} \in \mathbb{R}^{nd}$, then the maximum value of H is zero, which is achieved when all of the seeds are in the same place by (ii).

(viii) If there does not exist $\mathbf{X}^* \in \mathbb{D}_n$ such that $c_i(\mathbf{X}^*; \mathbf{v}) = b_i$, then ∇H is non-zero everywhere in \mathbb{D}_n . Therefore the maximum value of H on the compact set K is achieved either on the boundary of K or otherwise at a point in the interior of K where H is not differentiable, namely at a point in $K \setminus \mathbb{D}_n$.

□

Remark 4.3 (Consequences of Theorem 4.2 for Goal 2). Minimising the least squares error f is equivalent to minimising $|\nabla H|$ by equation (4.4). Assume that $\inf_{\mathbb{D}_n} f$ exists. Then, due to the invariance of ∇H under uniform translations and dilations of the seeds (equation (4.5)), we can restrict the minimisation problem (NLS) to a compact subset of \mathbb{D}_n :

$$\min_{\mathbf{X} \in \mathbb{D}_n} f(\mathbf{X}) = \min_{\mathbf{X} \in K \cap \mathbb{D}_n} f(\mathbf{X}) = \min_{\mathbf{X} \in K \cap \mathbb{D}_n} |\nabla H(\mathbf{X})|^2$$

for any compact set $K \subset \mathbb{R}^{nd}$ containing a neighbourhood of 0, or more generally a neighbourhood of a point of the form $(t, \dots, t) \in \mathbb{R}^{nd}$, $t \in \mathbb{R}^d$. For a suitable choice of compact convex set K , it turns out that maximising H on K (which is a convex optimisation problem) is equivalent to locally minimising $f = |\nabla H|^2$ on $K \cap \mathbb{D}_n$; see Section 4.4.

4.2 Goal 1: Uniqueness and construction of the solution

Definition 4.4 (Compatible diagrams). Given $(\mathbf{v}, \mathbf{B}) \in \mathcal{D}_n$, we say a Laguerre diagram $\{L_i(\mathbf{X}, \mathbf{v})\}_{i=1}^n$ is *compatible with the data* (\mathbf{v}, \mathbf{B}) if $c_i(\mathbf{X}; \mathbf{v}) = b_i$ for all $i \in \{1, \dots, n\}$. In other words, the diagram is compatible with the data (\mathbf{v}, \mathbf{B}) if the Laguerre cells have volumes v_i and centroids b_i .

The next result ensures us that if there exists a compatible diagram, then it is unique. Therefore Goal 1 has a unique solution (in the sense that the Laguerre cells are unique; the generators (\mathbf{X}, \mathbf{w}) are not unique by Lemma 2.1).

Theorem 4.5 (Uniqueness of compatible diagrams). *Let $(\mathbf{v}, \mathbf{B}) \in \mathcal{D}_n$. Suppose $\mathbf{X}, \mathbf{Y} \in \mathbb{D}_n$ are such that $\{L_i(\mathbf{X}; \mathbf{v})\}_{i=1}^n$ and $\{L_i(\mathbf{Y}; \mathbf{v})\}_{i=1}^n$ are compatible with the data (\mathbf{v}, \mathbf{B}) , i.e.,*

$$c_i(\mathbf{X}; \mathbf{v}) = c_i(\mathbf{Y}; \mathbf{v}) = b_i \quad \forall i \in \{1, \dots, n\}.$$

Then

$$L_i(\mathbf{X}; \mathbf{v}) = L_i(\mathbf{Y}; \mathbf{v}) \quad \forall i \in \{1, \dots, n\}.$$

In other words, a Laguerre tessellation is uniquely determined by the volumes and centroids of its cells.

Proof. Let $T^* : \Omega \rightarrow \mathbf{X}$ denote the optimal transport map between \mathcal{L}_Ω^d and $\nu(\mathbf{X}, \mathbf{v})$, i.e., $T(x) = x_i$ if $x \in \text{int } L_i(\mathbf{X}; \mathbf{v})$. Define a map $S : \Omega \rightarrow \mathbf{X}$ by

$$S(x) = x_i \quad \text{if } x \in \text{int } L_i(\mathbf{Y}; \mathbf{v}).$$

Since $\mathcal{L}_\Omega^d(S^{-1}(\{x_i\})) = \mathcal{L}_\Omega^d(L_i(\mathbf{Y}; \mathbf{v})) = v_i$, S is admissible for the transport problem between

\mathcal{L}_Ω^d and $\nu(X, \mathbf{v})$. Moreover,

$$\begin{aligned}
M(S) &= \int_\Omega |x - S(x)|^2 dx \\
&= \int_\Omega |x|^2 dx + \sum_{i=1}^n \int_{L_i(\mathbf{Y}; \mathbf{v})} (|x_i|^2 - 2x \cdot x_i) dx \\
&= \int_\Omega |x|^2 dx + \sum_{i=1}^n (v_i |x_i|^2 - 2v_i c_i(\mathbf{Y}; \mathbf{v}) \cdot x_i) \\
&= \int_\Omega |x|^2 dx + \sum_{i=1}^n (v_i |x_i|^2 - 2v_i c_i(\mathbf{X}; \mathbf{v}) \cdot x_i) \\
&= \int_\Omega |x|^2 dx + \sum_{i=1}^n \int_{L_i(\mathbf{X}; \mathbf{v})} (|x_i|^2 - 2x \cdot x_i) dx \\
&= \int_\Omega |x - T(x)|^2 dx \\
&= M(T^*).
\end{aligned}$$

Therefore S has the same transport cost as the optimal map T^* . Consequently, since the optimal transport map is unique (almost everywhere), $L_i(\mathbf{X}; \mathbf{v}) = L_i(\mathbf{Y}; \mathbf{v})$ for all $i \in \{1, \dots, n\}$, as required. \square

An immediate consequence of Theorems 4.2 and 4.5 is the following:

Theorem 4.6 (Goal 1 is a convex optimisation problem). *Let $\mathbf{X} \in \mathbb{D}_n$ and $\mathbf{w} \in \mathbb{R}^n$. For $i \in \{1, \dots, n\}$, define $v_i = m_i(\mathbf{X}, \mathbf{w})$ and $b_i = \xi_i(\mathbf{X}, \mathbf{w})$ to be the volume and centroid of the Laguerre cell $\text{Lag}_i(\mathbf{X}, \mathbf{w})$. Let $\mathbf{v} = (v_1, \dots, v_n)$ and $\mathbf{B} = (b_1, \dots, b_n)$. Then the concave function $H(\cdot; (\mathbf{v}, \mathbf{B}))$ achieves its maximum over \mathbb{R}^{nd} in \mathbb{D}_n . Let $\mathbf{Y} \in \mathbb{D}_n$ be any maximiser. Then*

$$L_i(\mathbf{Y}; \mathbf{v}) = L_i(\mathbf{X}; \mathbf{v}) \quad \forall i \in \{1, \dots, n\}.$$

In other words, we can recover a Laguerre tessellation from the volumes and centroids of its cells by solving a convex optimisation problem (maximising the concave function H in \mathbb{R}^{nd}).

Proof. Note that $\text{Lag}_i(\mathbf{X}, \mathbf{w}) = L_i(\mathbf{X}; \mathbf{v})$ and $\xi_i(\mathbf{X}, \mathbf{w}) = c_i(\mathbf{X}; \mathbf{v})$. The function $H(\cdot; (\mathbf{v}, \mathbf{B}))$ achieves its maximum over \mathbb{R}^{nd} at $\mathbf{X} \in \mathbb{D}_n$ because H is concave and $\nabla H(\mathbf{X}; (\mathbf{v}, \mathbf{B})) = 0$ by Theorem 4.2 (iv). If $\mathbf{Y} \in \mathbb{D}_n$ is any maximiser, then $\nabla H(\mathbf{Y}; (\mathbf{v}, \mathbf{B})) = 0$ and hence $c_i(\mathbf{Y}; \mathbf{v}) = b_i = c_i(\mathbf{X}; \mathbf{v})$. We conclude from Theorem 4.5 that $L_i(\mathbf{Y}; \mathbf{v}) = L_i(\mathbf{X}; \mathbf{v})$ for all $i \in \{1, \dots, n\}$, as required. \square

4.3 Goal 2: Existence of compatible diagrams

Now we turn our attention to Goal 2. We start with a special case; we seek necessary conditions on the data (\mathbf{v}, \mathbf{B}) for the existence of a compatible diagram, namely, for the minimum value of the fitting error (3.1) to be zero. In this case the compatible diagram can be found by maximising the concave function H , as described in the previous section. In Section 4.4 we will study the general case of Goal 2, where the minimum of the fitting error (3.1) is greater than zero.

Generically, for ‘typical’ data $(\mathbf{v}, \mathbf{B}) \in \mathcal{D}_n$ there does not exist a compatible diagram with cells with volumes v_i and centroids b_i , as the following example demonstrates.

Example 4.7 (Non-existence of a compatible diagram). Take $d = 1$, $\Omega = [0, 1]$, $n = 2$, $\mathbf{v} = (0.5, 0.5)$, $\mathbf{X} = (x_1, x_2) \in \mathbb{R}^2$ with $x_1 < x_2$. Then $L_1(\mathbf{X}; \mathbf{v}) = [0, 0.5]$ and $L_2(\mathbf{X}; \mathbf{v}) = [0.5, 1]$. (Note that this is true whatever the positions of x_1 and x_2 , as long as $x_1 < x_2$.) If the target centroids are $\mathbf{B} = (0.25, 0.75)$, then the diagram $\{L_i(\mathbf{X}; \mathbf{v})\}_{i=1}^2$ is compatible with (\mathbf{v}, \mathbf{B}) but, for any other choice of \mathbf{B} , there does not exist a compatible diagram.

Lemma 4.8 (Necessary condition for existence: minimum distance between centroids). *Let $(\mathbf{v}, \mathbf{B}) \in \mathcal{D}_n$ and suppose that there exists a Laguerre tessellation $\{L_i(\mathbf{X}; \mathbf{v})\}_{i=1}^n$ of Ω that is compatible with the data (\mathbf{v}, \mathbf{B}) . Then, for all $i \in \{1, \dots, n\}$,*

$$\text{dist}(c_i(\mathbf{X}; \mathbf{v}), \partial\Omega) = \text{dist}(b_i, \partial\Omega) \geq r_i, \quad (4.7)$$

where

$$r_i = \frac{v_i}{4\alpha_{d-1}} \left(\frac{\text{diam}(\Omega)}{2} \right)^{1-d}$$

and α_{d-1} is the volume of the unit ball in \mathbb{R}^{d-1} . Moreover, for all $i, j \in \{1, \dots, n\}$, $i \neq j$,

$$|c_i(\mathbf{X}; \mathbf{v}) - c_j(\mathbf{X}; \mathbf{v})| = |b_i - b_j| \geq r_i + r_j. \quad (4.8)$$

Proof. The idea for the proof comes from [37, Appendix A]. To prove (4.7) and (4.8), it suffices to show that

$$\text{dist}(b_i, \partial L_i(\mathbf{X}; \mathbf{v})) \geq r_i$$

for all $i \in \{1, \dots, n\}$. Let e_d be the d -th standard basis vector of \mathbb{R}^d . Without loss of generality (by rotating and translating Ω if necessary), we can assume that

$$L_i(\mathbf{X}; \mathbf{v}) \subseteq \{x \in \mathbb{R}^d : x \cdot e_d \geq 0\}$$

and

$$\text{dist}(b_i, \partial L_i(\mathbf{X}; \mathbf{v})) = b_i \cdot e_d.$$

Let $\Pi(\Omega)$ denote the projection of Ω onto the set $\{x \in \mathbb{R}^d : x \cdot e_d = 0\}$. There exists $s > 0$ such that

$$\begin{aligned} \frac{v_i}{2} &= \mathcal{L}^d(L_i(\mathbf{X}; \mathbf{v}) \cap \{x \in \mathbb{R}^d : x \cdot e_d \leq s\}) \\ &\leq s \mathcal{H}^{d-1}(\Pi(\Omega)) \\ &\leq s \alpha_{d-1} \left(\frac{\text{diam}(\Omega)}{2} \right)^{d-1} \end{aligned}$$

by the isodiametric inequality [26, Theorem 8.8] and the fact that $\text{diam}(\Pi(\Omega)) \leq \text{diam}(\Omega)$. By definition of r_i , we have $\frac{s}{2} \geq r_i$. Define

$$A = L_i(\mathbf{X}; \mathbf{v}) \cap \{x \in \mathbb{R}^d : x \cdot e_d \geq s\}.$$

Note that $\mathcal{L}^d(A) = v_i/2$. Then

$$b_i \cdot e_d = \frac{1}{v_i} \int_{L_i} x \cdot e_d \, dx \geq \frac{1}{v_i} \int_A x \cdot e_d \, dx \geq \frac{1}{v_i} \int_A s \, dx = \frac{s}{2} \geq r_i,$$

as desired. \square

If the domain Ω is a cuboid, then one can improve the bound (4.7) as follows.

Lemma 4.9 (Necessary condition for existence: distance of centroids from boundary). *Let $\Omega = [0, l_1] \times \cdots \times [0, l_d]$ and let b_i^j denote the j^{th} coordinate of the i^{th} target centroid. Let $(\mathbf{v}, \mathbf{B}) \in \mathcal{D}_n$ and suppose that there exists a Laguerre tessellation $\{L_i(\mathbf{X}; \mathbf{v})\}_{i=1}^n$ of Ω that is compatible with the data (\mathbf{v}, \mathbf{B}) . Then*

$$\frac{v_i l_j}{2\text{vol}(\Omega)} \leq b_i^j \leq l_j - \frac{v_i l_j}{2\text{vol}(\Omega)}.$$

In particular,

$$\text{dist}(c_i(\mathbf{X}; \mathbf{v}), \partial\Omega) = \text{dist}(b_i, \partial\Omega) \geq \min_j \frac{v_i l_j}{2\text{vol}(\Omega)}.$$

Proof. The inequalities are obtained by computing $H(\lambda \mathbf{e}_i^j)$ for suitable $\lambda \in \mathbb{R} \setminus \{0\}$, where $\mathbf{e}_i^j \in \mathbb{R}^{nd}$ denotes the $(d(i-1) + j)$ -th standard basis vector of \mathbb{R}^{nd} , for $i \in \{1, \dots, n\}$ and $j \in \{1, \dots, d\}$. If there exists a compatible diagram, then $H(\lambda \mathbf{e}_i^j) \leq 0$ by Theorem 4.2(vii). With this choice of seeds, $\mathbf{X} = \lambda \mathbf{e}_i^j$, there are only two distinct seeds (all the seeds are located at the origin except for the i -th seed, which has coordinates $x_i^j = 1$ and $x_i^k = 0$ for $k \neq j$) and hence $H(\mathbf{X})$ is easy to evaluate.

Assume without loss of generality that $i = 1$ and $j = 1$. In order to evaluate $H(\lambda \mathbf{e}_1^1)$, we need to compute $W_2^2(\mathcal{L}_\Omega^d, \nu(\mathbf{X}, \mathbf{v}))$, where $\nu(\mathbf{X}, \mathbf{v}) = v_1 \delta_{x_1} + (\text{vol}(\Omega) - v_1) \delta_0$ and $x_1 = (\lambda, 0, \dots, 0) \in \mathbb{R}^d$. The optimal transport map T^* partitions Ω into two cells, one of volume v_1 and the other of volume $\text{vol}(\Omega) - v_1$. The boundary between the two cells consists of the points $x \in \Omega$ satisfying the equation

$$|x - x_1|^2 - w \leq |x - 0|^2 \iff x \cdot (1, 0, \dots, 0) = \frac{\lambda^2 - w}{2\lambda}$$

for some $w \in \mathbb{R}$. Therefore the boundary is contained in the plane with normal vector $(1, 0, \dots, 0)$ and distance $\delta := (\lambda^2 - w)/(2\lambda)$ from the origin. The value of δ is determined by the volume constraints and the sign of λ . If $\lambda > 0$, then the Laguerre cell corresponding to the seed x_1 is $L_1 := [\delta, l_1] \times [0, l_2] \times \cdots \times [0, l_d]$, which has volume v_1 . Therefore

$$(l_1 - \delta) l_2 \cdots l_d = v_1 \iff \delta = l_1 - \frac{v_1}{l_2 \cdots l_d}.$$

Note that L_1 has centroid

$$c_1 := \left(\delta + \frac{l_1 - \delta}{2}, \frac{l_2}{2}, \dots, \frac{l_d}{2} \right) = \left(l_1 - \frac{v_1}{2l_2 \cdots l_d}, \frac{l_2}{2}, \dots, \frac{l_d}{2} \right).$$

Let $L_0 = [0, \delta] \times [0, l_2] \times \cdots \times [0, l_d]$ be the Laguerre cell corresponding to the seed 0. Then

$$\begin{aligned} H(\lambda \mathbf{e}_i^j) &= \frac{1}{2} \int_{L_1} |x - x_1|^2 dx + \frac{1}{2} \int_{L_0} |x - 0|^2 dx - \frac{1}{2} v_1 |x_1|^2 + v_1 x_1 \cdot b_1 - \frac{1}{2} \int_{\Omega} |x|^2 dx \\ &= v_1 x_1 \cdot (b_1 - c_1) \\ &= v_1 \lambda \left(b_1^1 - \left(l_1 - \frac{v_1}{2l_2 \cdots l_d} \right) \right). \end{aligned}$$

Since $\lambda > 0$,

$$H(\lambda \mathbf{e}_1^1) \leq 0 \iff b_1^1 \leq l_1 - \frac{v_1}{2l_2 \cdots l_d} = l_1 - \frac{v_1 l_1}{2\text{vol}(\Omega)},$$

as required. The other inequality, $b_1^1 \geq v_1 l_1 / (2\text{vol}(\Omega))$, can be derived analogously by taking $\lambda < 0$. \square

Lemma 4.10 (Necessary condition for existence: cyclical monotonicity). *Let $(\mathbf{v}, \mathbf{B}) \in \mathcal{D}_n$ and suppose that there exists a Laguerre tessellation $\{L_i(\mathbf{X}; \mathbf{v})\}_{i=1}^n$ of Ω that is compatible with the data (\mathbf{v}, \mathbf{B}) . Then the set $\{(b_i, x_i)\}_{i=1}^n$ is cyclically monotone, which means that for every index set $\mathcal{I} \subseteq \{1, \dots, n\}$ and every permutation σ of \mathcal{I} ,*

$$\sum_{i \in \mathcal{I}} b_i \cdot x_i \geq \sum_{i \in \mathcal{I}} b_i \cdot x_{\sigma(i)}.$$

In particular, by taking $\mathcal{I} = \{i, j\}$, it follows that

$$(b_i - b_j) \cdot (x_i - x_j) \geq 0$$

for all $i, j \in \{1, \dots, n\}$, $i \neq j$.

Proof. Let $T^* : \Omega \rightarrow \mathbf{X}$ denote the optimal transport map between \mathcal{L}_Ω^d and $\nu(\mathbf{X}, \mathbf{v})$. A standard result in optimal transport theory states that $T^* = \nabla u$ for some convex function $u : \Omega \rightarrow \mathbb{R}$ [47, Section 1.3.1]. Since $b_i = c_i(\mathbf{X}; \mathbf{v}) \in L_i(\mathbf{X}; \mathbf{v})$, then $T^*(b_i) = x_i$. Therefore the set $\{(b_i, x_i)\}_{i=1}^n = \{(b_i, T^*(b_i))\}_{i=1}^n = \{(b_i, \nabla u(b_i))\}_{i=1}^n$ is contained in the graph of the subdifferential of u . It follows that $\{(b_i, x_i)\}_{i=1}^n$ is cyclically monotone by Rockafellar's Theorem [46, p. 238, Theorem 24.8]. \square

As far as we are aware, it is an open problem to find sufficient conditions for the existence of compatible diagrams, that is, to find conditions on $(\mathbf{v}, \mathbf{B}) \in \mathcal{D}_n$ that guarantee that there exists a Laguerre diagram that is compatible with (\mathbf{v}, \mathbf{B}) .

4.4 Goal 2: Rewriting (NLS) as a convex optimisation problem

In this section we consider the general case of Goal 2. Our main theorem is the following.

Theorem 4.11 (Local minimisers of (NLS) can be found by convex optimisation). *Let $(\mathbf{v}, \mathbf{B}) \in \mathcal{D}_n$ be such that there does not exist a Laguerre diagram compatible with (\mathbf{v}, \mathbf{B}) . Fix $t \in \mathbb{R}^d$, $\mathbf{T} = (t, \dots, t) \in \mathbb{R}^{nd}$ and $R > 0$. Define $B \subset \mathbb{R}^{nd}$ to be the compact set $B = \{\mathbf{X} \in \mathbb{R}^{nd} : |\mathbf{X} - \mathbf{T}| \leq R\}$. Let $\mathbf{X}^* \in B$ be a global maximiser of the concave function H on B . Assume that $\mathbf{X}^* \in \mathbb{D}_n$, H is 3-times continuously differentiable in a neighbourhood of \mathbf{X}^* , and $\dim(\ker(D^2 H(\mathbf{X}^*))) = 1 + d$. Then \mathbf{X}^* is a local minimiser of f on \mathbb{D}_n . In particular, we can find local minimisers of the least squares error f by solving the convex optimisation problem $\max_B H$.*

Remark 4.12 (Assumptions of Theorem 4.11). The assumptions of Theorem 4.11 are implicit assumptions on the data (\mathbf{v}, \mathbf{B}) . We discuss each one in turn.

We only consider the case where there does not exist a Laguerre diagram compatible with (\mathbf{v}, \mathbf{B}) because the other case has already been covered in Theorem 4.6.

The assumption that $\mathbf{X}^* \in \mathbb{D}_n$, namely that the seeds are distinct, is restrictive and does not hold for all data $(\mathbf{v}, \mathbf{B}) \in \mathcal{D}_n$; see Section 5.2.2 for a numerical illustration. This

is explained in part in Remark 4.13; the first term of H (the optimal transport term) is maximised when all the seeds are in the same place. If the data (\mathbf{v}, \mathbf{B}) is such that the first term of H is the dominant term, then we expect some of the seeds in \mathbf{X}^* to coincide.

It can be shown using results from [20, 28] that H is 2-times continuously differentiable in \mathbb{D}_n . Expressions for the derivatives of the volumes and centroids of Laguerre cells with respect to the generators of the Laguerre tessellation can be read off from, e.g., [11, 17, 20, 28]. The assumption that H is 3-times continuously differentiable in a neighbourhood of \mathbf{X}^* is ‘generically’ true but may fail to hold if the diagram $\{L_i(\mathbf{X}^*; \mathbf{v})\}_{i=1}^n$ is ‘degenerate’ in the sense that there exists adjacent cells that intersect in a set of \mathcal{H}^{d-1} -measure zero (e.g., for $d = 2$, if four cells meet at a point, such as in a checkerboard configuration). In this case the combinatorics of some of the Laguerre cells (the number of faces, edges, vertices, etc.) may change in a neighbourhood of \mathbf{X}^* , and H may fail to be 3-times continuously differentiable.

We believe that the assumption $\dim(\ker(D^2H(\mathbf{X}^*))) = 1 + d$ is also ‘generically’ true, even if it is not always true. Due to the translation- and dilation-invariance of ∇H , we have $\dim(\ker(D^2H(\mathbf{X}))) \geq 1 + d$ for all $\mathbf{X} \in \mathbb{D}_n$. To see this, differentiate the expression $\nabla H(\lambda \mathbf{X}) = \nabla H(\mathbf{X})$ with respect to λ and set $\lambda = 1$ to obtain $D^2H(\mathbf{X})\mathbf{X} = 0$. Therefore $\mathbf{X} \in \ker(D^2H(\mathbf{X}))$. Similarly, let $e_i \in \mathbb{R}^d$ denote the i -th standard basis vector. Then differentiating $\nabla H(\mathbf{X} + s(e_i, \dots, e_i)) = \nabla H(\mathbf{X})$ with respect to s and setting $s = 0$ gives $(e_i, \dots, e_i) \in \ker(D^2H(\mathbf{X}))$ for all $i \in \{1, \dots, d\}$. Numerical evidence suggests that typically $\dim(\ker(D^2H(\mathbf{X}))) = 1 + d$, but it is possible to construct examples where $\dim(\ker(D^2H(\mathbf{X}))) > 1 + d$. For example, if a Laguerre cell L_i on the boundary of Ω only has one neighbour L_j (e.g., if L_i is a triangular Laguerre cell in the corner of a square domain), then the seed x_i and the weight w_i can be adjusted appropriately ($x_i \mapsto x_i + s(x_i - x_j)$, $s > 0$), while keeping the other seeds and weights fixed, without changing the Laguerre diagram, and hence without changing ∇H . This corresponds to another vector in the nullspace of D^2H .

Proof of Theorem 4.11. Let $\mathbf{X}^* = (x_1^*, \dots, x_n^*) \in B \cap \mathbb{D}_n$ be the global maximiser of H given in the statement of Theorem 4.11. Note that \mathbf{X}^* satisfies $|\mathbf{X}^* - \mathbf{T}| = R$ because of the following. If $|\mathbf{X}^* - \mathbf{T}| < R$, then $\nabla H(\mathbf{X}^*) = 0$ by the optimality of \mathbf{X}^* in B . But this contradicts the assumption that there does not exist a Laguerre diagram compatible with (\mathbf{v}, \mathbf{B}) .

The proof is split into three parts. Firstly, we write down the KKT conditions (first-order optimality conditions) for the optimisation problem $\max_B H$, which are satisfied by \mathbf{X}^* . Secondly, we use these conditions to show that $\nabla f(\mathbf{X}^*) = 0$. Finally, we show that \mathbf{X}^* is a local minimiser of f by checking the second-order, sufficient optimality conditions.

Let $c_{\text{ball}} : \mathbb{R}^{nd} \rightarrow \mathbb{R}$ be the constraint function given by $c_{\text{ball}}(\mathbf{X}) = R^2 - |\mathbf{X} - \mathbf{T}|^2$. Then $B = \{\mathbf{X} \in \mathbb{R}^{nd} : c_{\text{ball}}(\mathbf{X}) \geq 0\}$. By assumption, \mathbf{X}^* is a minimiser of $-H$ on B . The constraint $c_{\text{ball}} \geq 0$ is active at \mathbf{X}^* , which means that $c_{\text{ball}}(\mathbf{X}^*) = 0$. Observe that

$$\nabla c_{\text{ball}}(\mathbf{X}^*) = -2(\mathbf{X}^* - \mathbf{T}) \neq 0$$

because $\mathbf{X}^* \in \mathbb{D}_n$. Therefore \mathbf{X}^* satisfies the linear independence constraint qualification (LICQ) (see [41, Definition 12.4]) and so, by the Karush-Kuhn-Tucker Theorem [41, Theorem 12.1], there exists a Lagrange multiplier $\lambda^* \geq 0$ such that

$$-\nabla H(\mathbf{X}^*) = \lambda^* \nabla c_{\text{ball}}(\mathbf{X}^*) = -2\lambda^*(\mathbf{X}^* - \mathbf{T}). \quad (4.9)$$

Next we show that \mathbf{X}^* is a critical point of f . By equation (4.9),

$$\nabla f(\mathbf{X}^*) = 2D^2H(\mathbf{X}^*)\nabla H(\mathbf{X}^*) = 4\lambda^*D^2H(\mathbf{X}^*)(\mathbf{X}^* - \mathbf{T}) = 0$$

since \mathbf{X}^* and \mathbf{T} belong to $\ker(D^2H(\mathbf{X}^*))$; see Remark 4.12.

Finally, we show that \mathbf{X}^* is a local minimiser of f . To compute D^2f we will use the Einstein summation convention (sum over repeated indices), with subscript Roman indices corresponding to seeds and superscript Greek indices corresponding to components in \mathbb{R}^d . For example, x_i^α denotes component $\alpha \in \{1, \dots, d\}$ of seed $i \in \{1, \dots, n\}$. For all $i, j \in \{1, \dots, n\}$ and $\alpha, \beta \in \{1, \dots, d\}$,

$$\begin{aligned} \frac{\partial f}{\partial x_i^\alpha} &= 2 \frac{\partial^2 H}{\partial x_i^\alpha \partial x_k^\gamma} \frac{\partial H}{\partial x_k^\gamma}, \\ \frac{\partial^2 f}{\partial x_i^\alpha \partial x_j^\beta} &= 2 \frac{\partial^3 H}{\partial x_j^\beta \partial x_i^\alpha \partial x_k^\gamma} \frac{\partial H}{\partial x_k^\gamma} + 2 \frac{\partial^2 H}{\partial x_i^\alpha \partial x_k^\gamma} \frac{\partial^2 H}{\partial x_j^\beta \partial x_k^\gamma}, \end{aligned} \quad (4.10)$$

where k is summed over $\{1, \dots, n\}$ and γ is summed over $\{1, \dots, d\}$. Recall that for all $\mathbf{X} \in \mathbb{D}_n$, $D^2H(\mathbf{X})\mathbf{X} = 0$, i.e.,

$$\frac{\partial^2 H}{\partial x_i^\alpha \partial x_k^\gamma} x_k^\gamma = 0.$$

Differentiating with respect to x_j^β gives

$$\frac{\partial^3 H}{\partial x_j^\beta \partial x_i^\alpha \partial x_k^\gamma} x_k^\gamma + \frac{\partial^2 H}{\partial x_i^\alpha \partial x_j^\beta} = 0. \quad (4.11)$$

Evaluating (4.10) at \mathbf{X}^* and using (4.9) gives

$$\begin{aligned} \frac{\partial^2 f}{\partial x_i^\alpha \partial x_j^\beta}(\mathbf{X}^*) &= 4\lambda^* \frac{\partial^3 H}{\partial x_j^\beta \partial x_i^\alpha \partial x_k^\gamma}(\mathbf{X}^*) ((\mathbf{X}^*)_k^\gamma - (\mathbf{T})_k^\gamma) + 2 \frac{\partial^2 H}{\partial x_i^\alpha \partial x_k^\gamma}(\mathbf{X}^*) \frac{\partial^2 H}{\partial x_j^\beta \partial x_k^\gamma}(\mathbf{X}^*) \\ &= -4\lambda^* \frac{\partial^2 H}{\partial x_i^\alpha \partial x_j^\beta}(\mathbf{X}^*) + 2 \frac{\partial^2 H}{\partial x_i^\alpha \partial x_k^\gamma}(\mathbf{X}^*) \frac{\partial^2 H}{\partial x_j^\beta \partial x_k^\gamma}(\mathbf{X}^*), \end{aligned}$$

where in the second line we used (4.11) and the fact that $\mathbf{T} \in \ker(D^2H(\mathbf{X}^*))$. Therefore

$$D^2f(\mathbf{X}^*) = -4\lambda^* D^2H(\mathbf{X}^*) + 2 (D^2H(\mathbf{X}^*))^2. \quad (4.12)$$

Recall that $\lambda^* \geq 0$ and $D^2H(\mathbf{X}^*)$ is negative semi-definite (since H is concave). Therefore $D^2f(\mathbf{X}^*)$ is positive semi-definite. Moreover, if $\mathbf{Y} \in \mathbb{R}^{nd}$ satisfies $\mathbf{Y} \cdot D^2f(\mathbf{X}^*)\mathbf{Y} = 0$, then $\mathbf{Y} \in \ker(D^2H(\mathbf{X}^*))$, namely $\mathbf{Y} = a\mathbf{X}^* + (b, \dots, b)$ for some $a \in \mathbb{R}$, $b \in \mathbb{R}^d$; see Remark 4.12. But

$$f(\mathbf{X}^* + \mathbf{Y}) = f((1+a)\mathbf{X}^* + (b, \dots, b)) = f(\mathbf{X}^*)$$

by Theorem 4.2 (v). Therefore $\mathbf{Z} \cdot D^2f(\mathbf{X}^*)\mathbf{Z} > 0$ for all directions $\mathbf{Z} \in \mathbb{R}^{nd}$ except for those directions along which f is constant.

Let $\mathbf{Z} \in \mathbb{R}^{nd}$ and write $\mathbf{Z} = \mathbf{Y} + \mathbf{Y}^\perp$, where $\mathbf{Y} \in \ker(D^2H(\mathbf{X}^*))$ and \mathbf{Y}^\perp belongs to the orthogonal subspace of \mathbb{R}^{nd} . We will show that $f(\mathbf{X}^* + \mathbf{Z}) \geq f(\mathbf{X}^*)$ if $|\mathbf{Z}|$ is sufficiently small. We can assume that $\mathbf{Y}^\perp \neq 0$, otherwise $f(\mathbf{X}^* + \mathbf{Z}) = f(\mathbf{X}^*)$. By Taylor's Theorem there exists $t \in (0, 1)$ such that

$$f(\mathbf{X}^* + \mathbf{Z}) = f(\mathbf{X}^*) + \frac{1}{2} \mathbf{Z} \cdot D^2f(\mathbf{X}^* + t\mathbf{Z})\mathbf{Z}.$$

Note that

$$\mathbf{Z} \cdot D^2 f(\mathbf{X}^*) \mathbf{Z} = \mathbf{Y}^\perp \cdot D^2 f(\mathbf{X}^*) \mathbf{Y}^\perp > 0$$

since $\mathbf{Y}^\perp \neq 0$. Since $D^2 f$ is continuous, it follows that $\mathbf{Z} \cdot D^2 f(\mathbf{X}) \mathbf{Z} > 0$ for all \mathbf{X} in a sufficiently small neighbourhood of \mathbf{X}^* . Therefore $f(\mathbf{X}^* + \mathbf{Z}) > f(\mathbf{X}^*)$ if $|\mathbf{Z}|$ is sufficiently small. It follows that \mathbf{X}^* is a local minimiser of f , as required. \square

Remark 4.13 (Application of Theorem 4.11: Justification of the heuristic from [50]). A popular heuristic for fitting Laguerre diagrams to volume and centroid data (approximately solving $\min f$) is to take the seeds to be the target centroids, $\mathbf{X} = \mathbf{B}$; see for example [50]. We give a partial justification for this heuristic. We can decompose H as

$$H(\mathbf{X}) = F(\mathbf{X}) + G(\mathbf{X}), \quad \text{where} \quad G(\mathbf{X}) = -\frac{1}{2} \sum_{i=1}^n v_i |x_i|^2 + \sum_{i=1}^n v_i x_i \cdot b_i - \frac{1}{2} \int_{\Omega} |x|^2 dx$$

and F was defined in (4.2). Consider maximising H over $B = \{\mathbf{X} \in \mathbb{R}^{nd} : |\mathbf{X} - \mathbf{T}| \leq R\}$, where $\mathbf{T} = (\sigma(\Omega), \dots, \sigma(\Omega))$ and $\sigma(\Omega)$ is the centroid of Ω . This is equivalent to locally minimising the fitting error f by Theorem 4.11. The maximiser of H depends on the competition between the terms F and G . It can be shown that the first term, F , is maximised when all the seeds coincide and are as far from the centroid of Ω as possible, namely when $\mathbf{X} = (x_1, \dots, x_1) \in \partial B$. This is because maximising F is equivalent to finding the worst approximation of the Lebesgue measure by a discrete measure in the Wasserstein metric. On the other hand, the second term, G , is globally maximised over \mathbb{R}^{nd} by $\mathbf{X} = \mathbf{B}$, namely when the seeds are the target centroids. This is the heuristic from [50]. If the second term dominates, then we would expect the maximiser of H (and the minimiser of f) to be close to \mathbf{B} . This partially justifies the heuristic used by [50] and other authors. On the other hand, if the first term dominates, then the maximiser of H may not belong to \mathbb{D}_n . This partially explains the numerical observations given in Section 5.2.2.

Remark 4.14 (The set K should be a ball). In Theorem 4.11 it is important that the set B where we maximise H is a ball. By Theorem 4.2 (v), if the infimum of f is attained, we have $\min_{\mathbb{D}_n} f = \min_{K \cap \mathbb{D}_n} f$ for any compact set K containing a neighbourhood of a point of the form $\mathbf{T} = (t, \dots, t) \in \mathbb{R}^{nd}$, not just for balls. However, we cannot replace the ball B by an arbitrary compact set K in the statement of Theorem 4.11. The fact that H is 1-positively homogeneous is also important. In general, it is not true that the maximiser of a concave function on a compact set is a minimiser of the norm of its gradient. For example, let $g : \mathbb{R}^2 \rightarrow \mathbb{R}$ be the concave function $g(x) = -\frac{1}{2}(x_1 - 2)^2 - 2(x_2 - 1)^2$. Let $c : \mathbb{R}^2 \rightarrow \mathbb{R}$ be the constraint function $c(x) = 1 - \left(\frac{x_1}{2}\right)^2 - x_2^2$ and S be the ellipse $S = \{x \in \mathbb{R}^2 : c(x) \geq 0\}$. It can be shown that the global maximiser of g on S is $x^* = (\sqrt{2}, 1/\sqrt{2}) \in \partial S$, but the global minimiser of the convex function $|\nabla g|^2$ on S is $y^* = (2y_2/(4 - 3y_2), y_2) \in \partial S$ with $y_2 = \frac{1}{3}(2 - \sqrt{5} + \sqrt{3 + 2\sqrt{5}}) \approx (1.108097, 0.832484)$. Note that $y^* \neq x^*$.

We include the following theorem since it may be of general interest in convex optimisation. It gives conditions under which minimising a 1-positively homogeneous convex function on a ball is equivalent to locally minimising the norm of its gradient. We do not include its proof since it is very similar to the proof of Theorem 4.11.

Theorem 4.15 (Minimising the norm of the gradient of a convex function). *Let $g : \mathbb{R}^n \rightarrow \mathbb{R}$ be convex. Suppose that there exists $x_0 \in \mathbb{R}^n$ such that, for all $\lambda > 0$, $x \in \mathbb{R}^n$,*

$$g(\lambda(x - x_0) + x_0) = \lambda g(x). \quad (4.13)$$

(If $x_0 = 0$, then g is 1-positively homogeneous.) Assume that g is continuously differentiable on $\mathbb{R}^n \setminus \{x_0\}$. Let $R > 0$ and $B_R = \{x \in \mathbb{R}^n : |x - x_0| \leq R\}$. Assume that the global minimum of g on B_R is achieved at a point $x^ \in \partial B_R$. Moreover, assume that g is 3-times continuously differentiable in a neighbourhood of x^* and $\ker(D^2g(x^*)) = \text{span}_{\mathbb{R}}\{x^* - x_0\}$. Then x^* is a local minimiser of $|\nabla g|$ on $\mathbb{R}^n \setminus \{x_0\}$.*

5 Numerical experiments

In this section we provide numerical experiments to illustrate the theory from Section 4.

5.1 Recovering a Laguerre diagram from the areas and centroids of its cells

First we show how to achieve Goal 1 using Theorem 4.2. In particular, we reconstruct a 2D Laguerre diagram given the areas and centroids of its cells by maximising H .

We take $\Omega = [0, 1]^2$, $n = 20$, we draw the seeds $\mathbf{X}_0 \in \Omega^n$ at random from the uniform distribution on Ω , and we set all the weights to be zero, $\mathbf{w}_0 = (0, \dots, 0)$, so that $(\mathbf{X}_0, \mathbf{w}_0)$ generates a Voronoi tessellation of Ω . For $i \in \{1, \dots, n\}$, we define v_i to be the area of $\text{Lag}_i(\mathbf{X}_0, \mathbf{w}_0)$ and b_i to be the centroid of $\text{Lag}_i(\mathbf{X}_0, \mathbf{w}_0)$. By Theorem 4.2 (iv), we can recover the Voronoi diagram $\{\text{Lag}_i(\mathbf{X}_0, \mathbf{w}_0)\}_{i=1}^n$ from (\mathbf{v}, \mathbf{B}) by numerically maximising the concave function H .

For numerical robustness, since Laguerre diagrams are only defined if the seeds are distinct, we found that it was necessary to maximise H subject to the constraint that the pairwise distance between the seeds is not too small, namely, that $c_{ij}(\mathbf{X}) \geq 0$ for all $i, j \in \{1, \dots, n\}$, $i < j$, where $c_{ij} : \mathbb{R}^{nd} \rightarrow \mathbb{R}$ are defined by

$$c_{ij}(\mathbf{X}) = |x_i - x_j|^2 - \delta^2,$$

where we take $\delta = 10^{-3}$ in all the experiments below. Without this constraint, an iterative numerical optimisation algorithm may produce an iterate with seeds very close together. As a very simple example, consider two seeds in one-dimension. If the initial guess has the seeds in the wrong order, then any convergent numerical optimisation algorithm would reorder the seeds, which may cause the seeds to get very close together as they swap positions. This could give rise to some numerical instability since it is difficult to compute Laguerre diagrams and solve optimal transport problems when the seeds are very close together. We have observed the analogue of this behaviour in two dimensions.

In addition, we impose the constraint $c_{\text{ball}}(\mathbf{X}) \geq 0$, where $c_{\text{ball}} : \mathbb{R}^{nd} \rightarrow \mathbb{R}$ is defined by

$$c_{\text{ball}}(\mathbf{X}) = R^2 - \sum_{i=1}^n |x_i - \sigma(\Omega)|^2, \quad R = \sqrt{\text{area}(\Omega) \cdot n},$$

and where $\sigma(\Omega)$ is the centroid of Ω . This constraint ensures that \mathbf{X} lies in the ball in \mathbb{R}^{nd} of radius R and centre $(\sigma(\Omega), \dots, \sigma(\Omega))$. In particular, it reduces the domain of the optimisation problem to a compact set. This can be done without loss of generality by Lemma 2.1.

In summary, we recover $\{\text{Lag}_i(\mathbf{X}_0, \mathbf{w}_0)\}_{i=1}^n$ from (\mathbf{v}, \mathbf{B}) by numerically solving the following constrained optimisation problem:

$$\max \left\{ H(\mathbf{X}; (\mathbf{v}, \mathbf{B})) : \mathbf{X} \in \mathbb{R}^{nd}, c_{\text{ball}}(\mathbf{X}) \geq 0, c_{ij}(\mathbf{X}) \geq 0 \forall i, j \in \{1, \dots, n\}, i < j \right\}. \quad (5.1)$$

Note that the maximum value is 0 by Theorem 4.2 (vii). As described above, we added the constraints $c_{ij} \geq 0$ for numerical stability. The price to pay is that the optimisation problem is no longer convex (the constraint set is not convex). An alternative approach, to preserve convexity, would be to maximise H over the convex set $\{c_{\text{ball}} \geq 0\}$ using a method for non-smooth convex optimisation (such as a proximal method) that does not need ∇H to be well-defined everywhere (note that H can be evaluated in a robust way even if the seeds are not distinct).

We solved the optimisation problem (5.1) in Python. To compute Laguerre diagrams and solve the semi-discrete optimal transport problem we used the Python library *pysdot* [3] (to compute $\mathbf{w}^*(\mathbf{X}; \mathbf{v})$). The initial guess for the optimal transport solver was generated using the rescaling method from [39, Section 2.2], which is based on Lemma 2.1. The optimal transport algorithm (the damped Newton method [28]) was terminated when the percentage error of the areas of the Laguerre cells fell below 0.1%, namely, when \mathbf{w} was such that

$$100 \cdot \frac{|m_i(\mathbf{X}, \mathbf{w}) - v_i|}{v_i} < 0.1 \quad \forall i \in \{1, \dots, n\}.$$

We used the Python function *scipy.optimize.minimize* to solve the constrained optimisation problem 5.1 with a random initial guess \mathbf{X}_{init} (drawn from the uniform distribution on Ω^{nd}), with the optimisation method *SLSQP*, and with the tolerance parameter *ftol* equal to $10^{-10}|H(\mathbf{X}_{\text{init}})|$.

The results are shown in Figures 1 and 2. The optimisation algorithm terminated successfully after 229 iterations. Figure 1, left, shows the Laguerre tessellation $\{L_i(\mathbf{X}_{\text{init}}; \mathbf{v})\}_{i=1}^n$ generated by the random initial guess \mathbf{X}_{init} , and Figure 1, right, shows the final Laguerre tessellation after 229 iterations. The red dots are the actual centroids, which are almost indistinguishable from the blue dots, the target centroids \mathbf{B} . Figure 2 shows the convergence of H and F to 0.

5.2 Fitting a Laguerre diagram to synthetic data

In this section we consider Goal 2. We fit a Laguerre tessellation to synthetic data that is obtained by perturbing a Voronoi diagram. We created the synthetic data as follows. First we took the Voronoi diagram $\{\text{Lag}_i(\mathbf{X}_0, \mathbf{w}_0)\}_{i=1}^n$ from Section 5.1 and computed the areas and centroids of its cells, (\mathbf{v}, \mathbf{B}) . Then we perturbed each centroid b_i by a random vector

$$u_i^\varepsilon = \varepsilon r_i (\cos \theta_i, \sin \theta_i),$$

where r_i is drawn from the uniform distribution on $[0, 1]$, θ_i is drawn from the uniform distribution on $[0, 2\pi]$, and $\varepsilon > 0$ is the size of the perturbation. Finally, so that the synthetic data is compatible (belongs to the set \mathcal{D}_n), we define

$$b_i^\varepsilon = b_i + u_i^\varepsilon + \left(\sigma(\Omega) - \frac{1}{\text{area}(\Omega)} \sum_{i=1}^n v_i (b_i + u_i^\varepsilon) \right),$$

where $\sigma(\Omega) = (1/2, 1/2)$ is the centroid of $\Omega = [0, 1]^2$. Then $(\mathbf{v}, \mathbf{B}^\varepsilon) \in \mathcal{D}_n$ is our synthetic data.

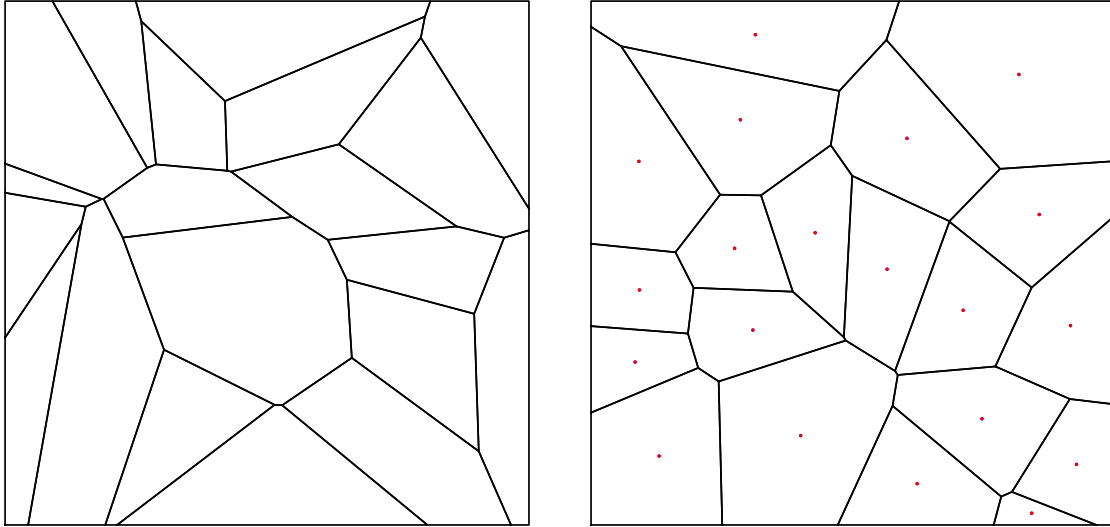


Figure 1: Recovering a Laguerre diagram $\{\text{Lag}_i(\mathbf{X}_0, \mathbf{w}_0)\}_{i=1}^n$ from the areas \mathbf{v} and centroids \mathbf{B} of its cells; see Section 5.1. Left: The Laguerre tessellation $\{L_i(\mathbf{X}_{\text{init}}; \mathbf{v})\}_{i=1}^n$ with cells of areas \mathbf{v} (up to a 0.1% error) generated from a random collection of seeds \mathbf{X}_{init} . Right: Numerical approximation of the unique Laguerre tessellation with cells of areas \mathbf{v} and centroids \mathbf{B} . This figure shows the Laguerre tessellation corresponding to an approximate maximiser of the constrained optimisation problem (5.1), computed by `scipy.optimize.minimize` using the initial guess \mathbf{X}_{init} and 229 iterations. The red dots are the centroids of the computed Laguerre cells. The blue dots (which are almost indistinguishable from the red dots) are the target centroids \mathbf{B} . The cells have areas \mathbf{v} up to a 0.1% error. We have not plotted the true Laguerre diagram $\{\text{Lag}_i(\mathbf{X}_0, \mathbf{w}_0)\}_{i=1}^n$ since it is indistinguishable from the computed Laguerre diagram.

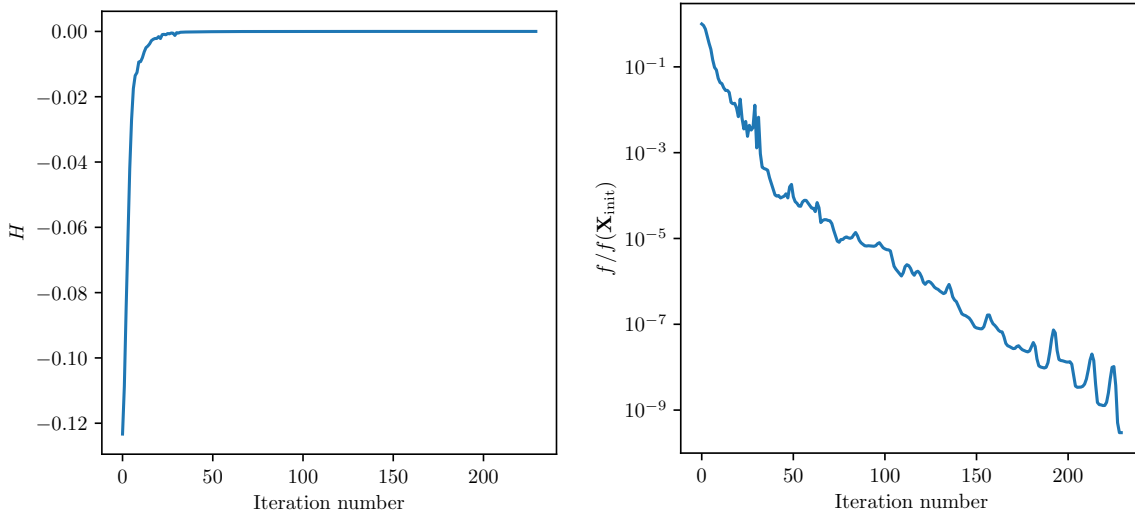


Figure 2: Recovering a Laguerre diagram – convergence of the algorithm from Section 5.1. Left: The value of the objective function H converges to its maximum value of 0. Right: The nonlinear least squares error f also converges to 0.

5.2.1 Small perturbations

First we considered a very small perturbation $\varepsilon = 0.001$. We fitted a Laguerre tessellation to the perturbed data $(\mathbf{v}, \mathbf{B}^\varepsilon)$ by solving the constrained optimisation problem (5.1) as described above in Section 5.1, with the same values of δ , R and $ftol$, but with the initial guess $\mathbf{X}_{\text{init}} = \mathbf{B}^\varepsilon$ (see Remark 4.13 for a justification for using this initial guess).

The algorithm terminated successfully after 402 iterations. The results are shown in Figures 3, 4 and 5, left. Figure 3, left, shows the Laguerre tessellation $\{L_i(\mathbf{X}_{\text{init}}; \mathbf{v})\}_{i=1}^n$ generated by the initial guess $\mathbf{X}_{\text{init}} = \mathbf{B}^\varepsilon$, and Figure 3, right, shows the final Laguerre tessellation after 402 iterations. The red dots are the actual centroids and the blue dots are the target centroids \mathbf{B}^ε . Since the perturbation is so small, the red and blue dots are almost indistinguishable. There are some minor visible differences between the Laguerre tessellation fitted to the unperturbed data (Figure 1, right) and the Laguerre tessellation fitted to the perturbed data (Figure 3, right).

As discussed in Remark 4.13, the initial guess $\mathbf{X}_{\text{init}} = \mathbf{B}^\varepsilon$ is a good approximation of the maximiser of (5.1), at least in the eyeball metric – compare Figure 3, left, to Figure 3, right. On the other hand, from Figure 4 we see that the final value of least squares error f is over three orders of magnitude smaller than $f(\mathbf{X}_{\text{init}})$. The objective function H increases from about -5×10^{-5} to 2.5×10^{-4} . Note that the maximum value of H is positive because there does not exist a Laguerre diagram with cells of areas and centroids $(\mathbf{v}, \mathbf{B}^\varepsilon)$. Since H can now take positive values, the constraint $c_{\text{ball}} \geq 0$ in (5.1) is necessary to ensure that the objective function is bounded by Theorem 4.2 (v).

Figure 5, left, shows the minimum distance between the seeds at each iteration, normalised by δ , which is the minimum distance between the seeds allowed by the constraint $c_{ij} \geq 0$. The dashed line corresponds to the constraint being active for some i, j . We see that the constraint becomes active around iteration 100, as the seeds rearrange themselves, but by the end of the simulation the seeds are well separated, at least 30 units of δ apart. This suggests that the maximum value of H on the ball $\{c_{\text{ball}} \geq 0\}$ is achieved at a point where all the seeds are distinct.

5.2.2 Larger perturbations

We repeated the simulations from the previous section with a slightly larger perturbation, $\varepsilon = 0.05$. The algorithm terminated successfully after 301 iterations and the results are shown in Figures 6, 7 and 5, right.

Figure 6 shows the initial (left) and final (right) Laguerre tessellations, with the target centroids \mathbf{B}^ε in blue and the centroids of the fitted diagram in red. This time there is a clear visible difference between the target and actual centroids, although the fit is still quite good. However, the fitted diagram (Figure 6, right) is somewhat ‘irregular’; some of the cells are rather elongated and there is a tendency for some of the edges of the Laguerre cells to align. This suggests that the methods proposed in this paper of maximising H /minimising f may not be entirely suitable for generating synthetic microstructures. It does, however, appear to work well for recovering Laguerre diagrams (Section 5.1) and fitting Laguerre diagrams to EBSD data (Section 5.3).

The convergence of H and F are illustrated in Figure 7. Figure 5, right, shows that at least one of the constraints $c_{ij} \geq 0$ is active at the final iteration (and from iteration 100 onwards). This suggests that, without the constraint $c_{ij} \geq 0$, some of the seeds would collide.

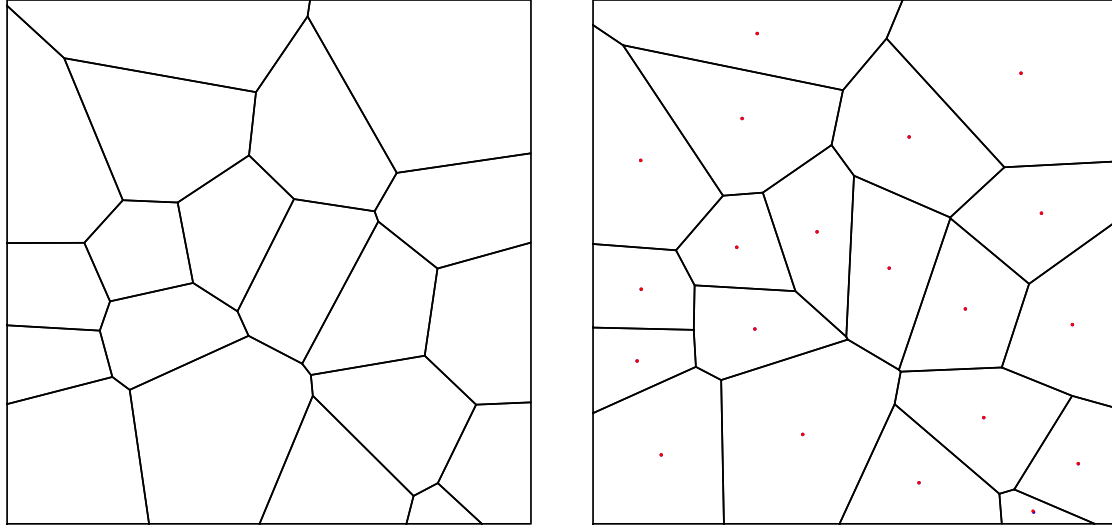


Figure 3: Fitting a Laguerre diagram to synthetic data $(\mathbf{v}, \mathbf{B}^\varepsilon)$ with $\varepsilon = 0.001$ (small perturbation); see Section 5.2.1. Left: The initial guess $\{L_i(\mathbf{X}_{\text{init}}; \mathbf{v})\}_{i=1}^n$ for the maximiser of (5.1), where $\mathbf{X}_{\text{init}} = \mathbf{B}^\varepsilon$. Right: An approximate maximiser of the constrained optimisation problem (5.1), computed by `scipy.optimize.minimize` using the initial guess \mathbf{X}_{init} and 402 iterations. The centroids of the Laguerre cells (red dots) are almost indistinguishable from the target centroids (blue dots).

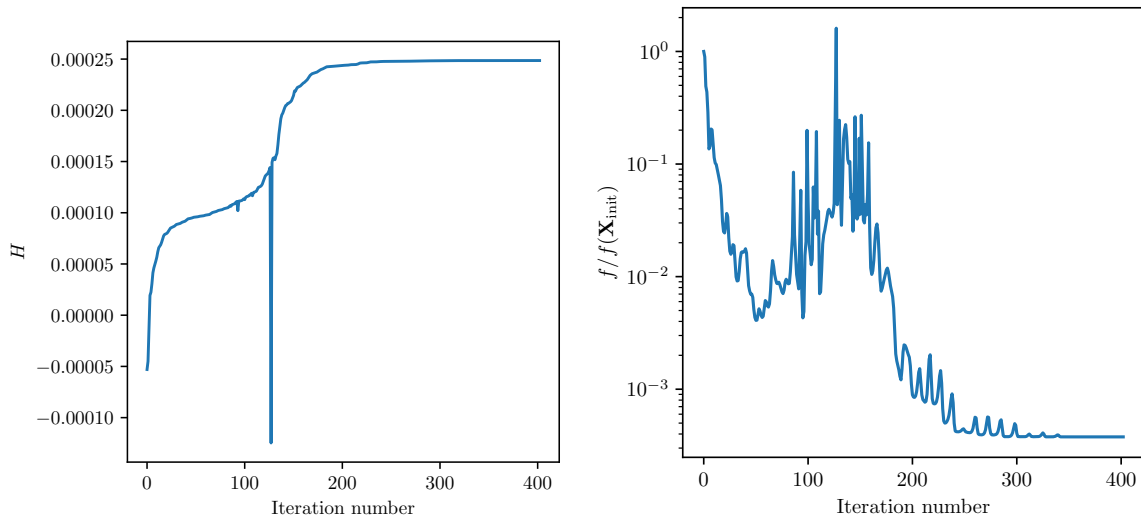


Figure 4: Fitting a Laguerre diagram to synthetic data (small perturbation) - convergence of the algorithm from Section 5.2.1. Left: Convergence of the objective function H . It converges to a positive value because there does not exist a Laguerre diagram with cells of areas and centroids $(\mathbf{v}, \mathbf{B}^\varepsilon)$. Right: Convergence of the least squares error f . The y -axis shows the ratio of the value of f at each iteration to its initial value $f(\mathbf{X}_{\text{init}})$.

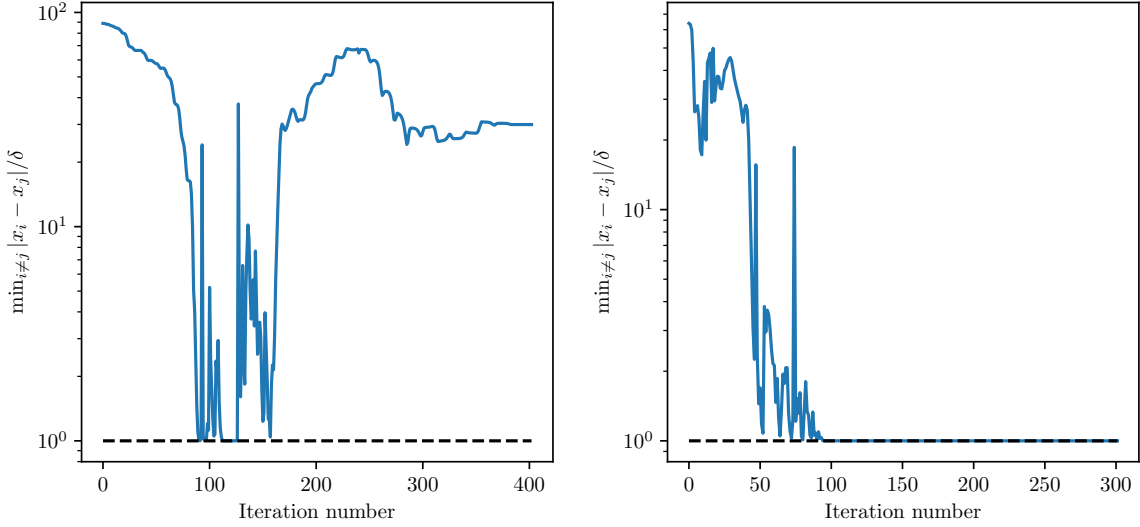


Figure 5: Fitting a Laguerre diagram to synthetic data (see Section 5.2) - minimum distance between the seeds for $\varepsilon = 0.001$ (left) and $\varepsilon = 0.05$ (right). The minimum distance between the seeds is normalised by the minimum allowed distance $\delta = 10^{-3}$. The dotted line corresponds to when at least one of the constraints $c_{ij} \geq 0$ is active. Left (small perturbation): At the end of the algorithm none of the constraints are active. The minimum distance between the seeds is at least 30δ . Right (larger perturbation): At the end of the algorithm at least one of the constraints is active. This suggests that if we solved (5.1) without the constraints $c_{ij} \geq 0$, then some of the seeds would collide.

In other words, it suggests that the maximum value of H in the set $\{c_{\text{ball}} \geq 0\}$ is achieved at a point where some of the seeds coincide. Therefore the assumptions of Theorem 4.11 are not satisfied, and there is no rigorous correspondence between maximising H and finding local minimisers of the least squares error f . Nevertheless, Figure 7 suggests that maximising H still works reasonably well at minimising f in practice. Moreover, we repeated this experiment by directly minimising f (using the approach described in the following section, by solving (5.2)) and obtained very similar results.

5.3 Fitting a Laguerre diagram to EBSD data

In this section we fit a Laguerre tessellation to an EBSD image provided by Tata Steel Research & Development. Figure 8, top, is an EBSD image of a single-phase steel. The pixels are coloured according to their crystallographic orientation. The orientation map is piecewise constant, and regions of constant orientation are known as *grains*. There are $n = 243$ grains in the image. From this image we extracted the areas \mathbf{v} and the centroids \mathbf{B} of the grains by counting the pixels in each grain. The domain is $\Omega = [0, 252.25]^2$ (measured in microns).

To fit a Laguerre tessellation to the EBSD data (\mathbf{v}, \mathbf{B}) we initially tried solving (5.1). However, as in Section 5.2.2, our experiments suggested that the maximum value of H on the ball $\{c_{\text{ball}} \geq 0\}$ is achieved at a point where some of the seeds coincide. Since Theorem 4.11 does not apply in this case, we decided to directly minimise f , rather than maximise H . To

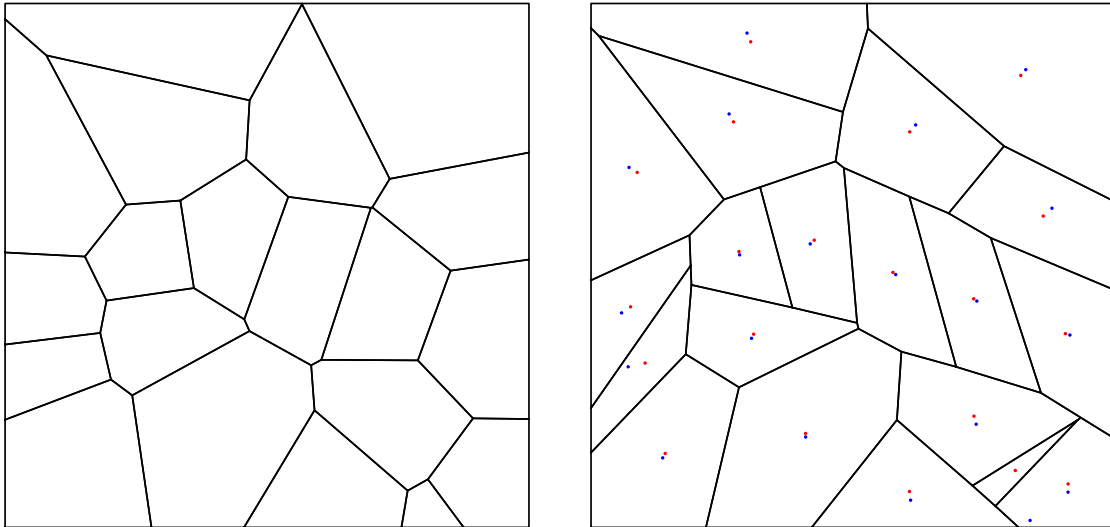


Figure 6: Fitting a Laguerre diagram to synthetic data $(\mathbf{v}, \mathbf{B}^\varepsilon)$ with $\varepsilon = 0.05$ (larger perturbation); see Section 5.2.2. Left: The initial guess $\{L_i(\mathbf{X}_{\text{init}}; \mathbf{v})\}_{i=1}^n$ for the maximiser of (5.1), where $\mathbf{X}_{\text{init}} = \mathbf{B}^\varepsilon$. Right: An approximate maximiser of the constrained optimisation problem (5.1), computed by `scipy.optimize.minimize` using the initial guess $\mathbf{X}_{\text{init}} = \mathbf{B}^\varepsilon$ and 301 iterations. The centroids of the Laguerre cells are in red and the target centroids are in blue. The centroid error is relatively small, but the Laguerre cells are not very ‘regular’. In our simulations we found that fitting a diagram to synthetic data tends to produce some elongated cells or cells that are aligned (have almost parallel edges), as seen here.

be precise, we solved the constrained optimisation problem

$$\min \left\{ \frac{n^2}{\text{area}(\Omega)^3} f(\mathbf{X}; (\mathbf{v}, \mathbf{B})) : \mathbf{X} \in \mathbb{R}^{nd}, c_{ij}(\mathbf{X}) \geq 0 \forall i, j \in \{1, \dots, n\}, i < j \right\}. \quad (5.2)$$

The normalisation factor $n^2/\text{area}(\Omega)^3$ is simply included so that objective function is non-dimensional and scales roughly constantly with respect to n (this is based on the assumption the cells have roughly equal area). The constraints $c_{ij} \geq 0$ are included as above for numerical robustness and to stop seeds colliding. Since F is invariant under dilations and translations, we do not need to include the constraint $c_{\text{ball}} \geq 0$.

We solved (5.2) using `scipy.optimize.minimize` with the initial guess $\mathbf{X}_{\text{init}} = \mathbf{B}$ and with the tolerance parameter `ftol` equal to $10^{-8}n^2f(\mathbf{X}_{\text{init}})/\text{area}(\Omega)^3 = 1.6308 \times 10^{-10}$.

The results are shown in Figures 8 and 9. The optimisation algorithm terminated successfully after 714 iterations. Figure 8, bottom-right, shows the Laguerre cells together with the centroids \mathbf{B} of the grains from the EBSD image in blue and the centroids of the fitted Laguerre cells in red. Figure 8, bottom-left, shows the fitted Laguerre diagram overlaid over the EBSD image. The quality of the fit is limited by the polygonal shape of the cells; in reality the grains may not be polygonal, as can be seen from the EBSD image in Figure 8 (top). Nevertheless, there is a clear resemblance, even though we are only minimising the least squares centroid error f , rather than the mismatch between the two figures (such as the number of misassigned pixels). Figure 9, left, shows the convergence of the algorithm.

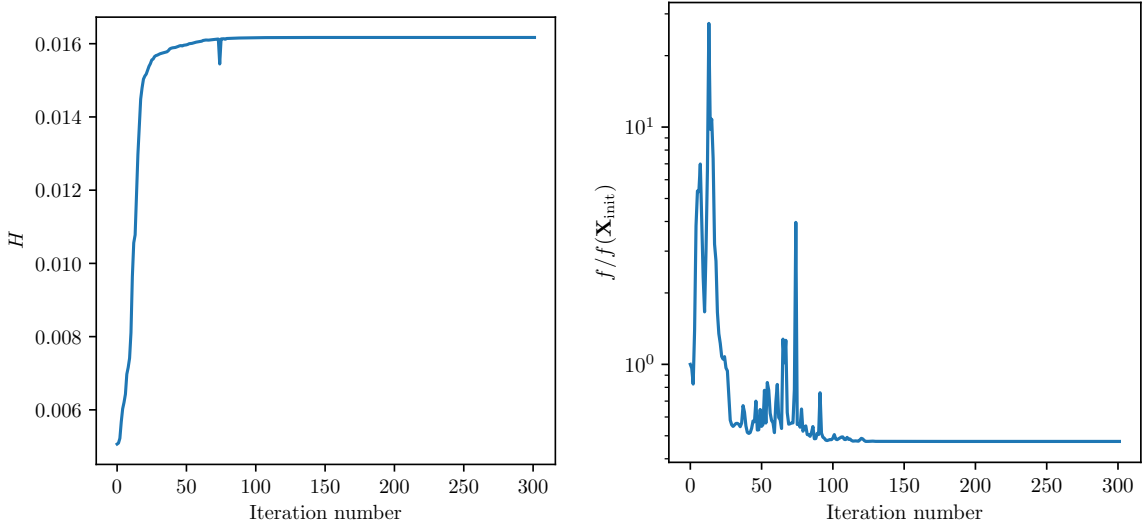


Figure 7: Fitting a Laguerre diagram to synthetic data (larger perturbation) - convergence of the algorithm from Section 5.2.2. Left: Convergence of the objective function H . Right: Convergence of the least squares error f . The y -axis shows the ratio of the value of f at each iteration to its initial value $f(\mathbf{X}_{\text{init}})$. We see that the initial guess $\mathbf{X}_{\text{init}} = \mathbf{B}^\varepsilon$ is very good; the optimisation algorithm only decreases the least squares error f by a factor of about 0.5 (after initially increasing it significantly).

The ratio of the initial value of f to the final value of f is 25.2. Figure 9, right, shows the minimum distance between the seeds, normalised by δ (the minimum distance between the seeds allowed by the constraints $c_{ij} \geq 0$). This suggests that $\inf\{f(\mathbf{X}; (\mathbf{v}, \mathbf{B})) : \mathbf{X} \in \mathbb{D}_n\}$ is not attained (seeds collide along an infimising sequence), which is why we introduced the constraints $c_{ij} \geq 0$ in (5.2).

6 Generalisation to anisotropic Laguerre tessellations

In this section we generalise some of our results to *anisotropic Laguerre tessellations* (also known as *anisotropic power diagrams* or *generalised balanced power diagrams*), which have recently been used to model polycrystalline materials, e.g., [7, 4, 48, 50, 43, 6, 5, 27, 19].

Definition 6.1 (Anisotropic Laguerre tessellations). Let $\mathbf{A} = (A_1, \dots, A_n)$ be a tuple of d -dimensional, symmetric, positive-definite matrices $A_i \in \mathbb{R}^{d \times d}$. Let $\mathbf{X} \in \mathbb{D}_n$ and $\mathbf{w} \in \mathbb{R}^n$. The i^{th} *anisotropic Laguerre cell* generated by $(\mathbf{X}, \mathbf{w}, \mathbf{A})$ is defined by

$$\text{Lag}_i^{\mathbf{A}}(\mathbf{X}, \mathbf{w}) = \{x \in \Omega : |x - x_i|_{A_i}^2 - w_i \leq |x - x_j|_{A_j}^2 - w_j \forall j \in \{1, \dots, n\}\}, \quad (6.1)$$

where $|\cdot|_{A_i}$ denotes the norm generated by A_i , which is defined by $|x|_{A_i} = (x \cdot A_i x)^{1/2}$ for all $x \in \mathbb{R}^d$. The *anisotropic Laguerre tessellation* generated by $(\mathbf{X}, \mathbf{w}, \mathbf{A})$ is the collection of cells $\{\text{Lag}_i^{\mathbf{A}}(\mathbf{X}, \mathbf{w})\}_{i=1}^n$.

The standard Laguerre tessellation is recovered by setting $A_i = I_d$ for all i , where I_d is the $d \times d$ identity matrix. The matrices A_i allow for some control over the aspect ratios of the cells. If $d = 2$ each edge of an anisotropic Laguerre cell is an arc of a conic section.

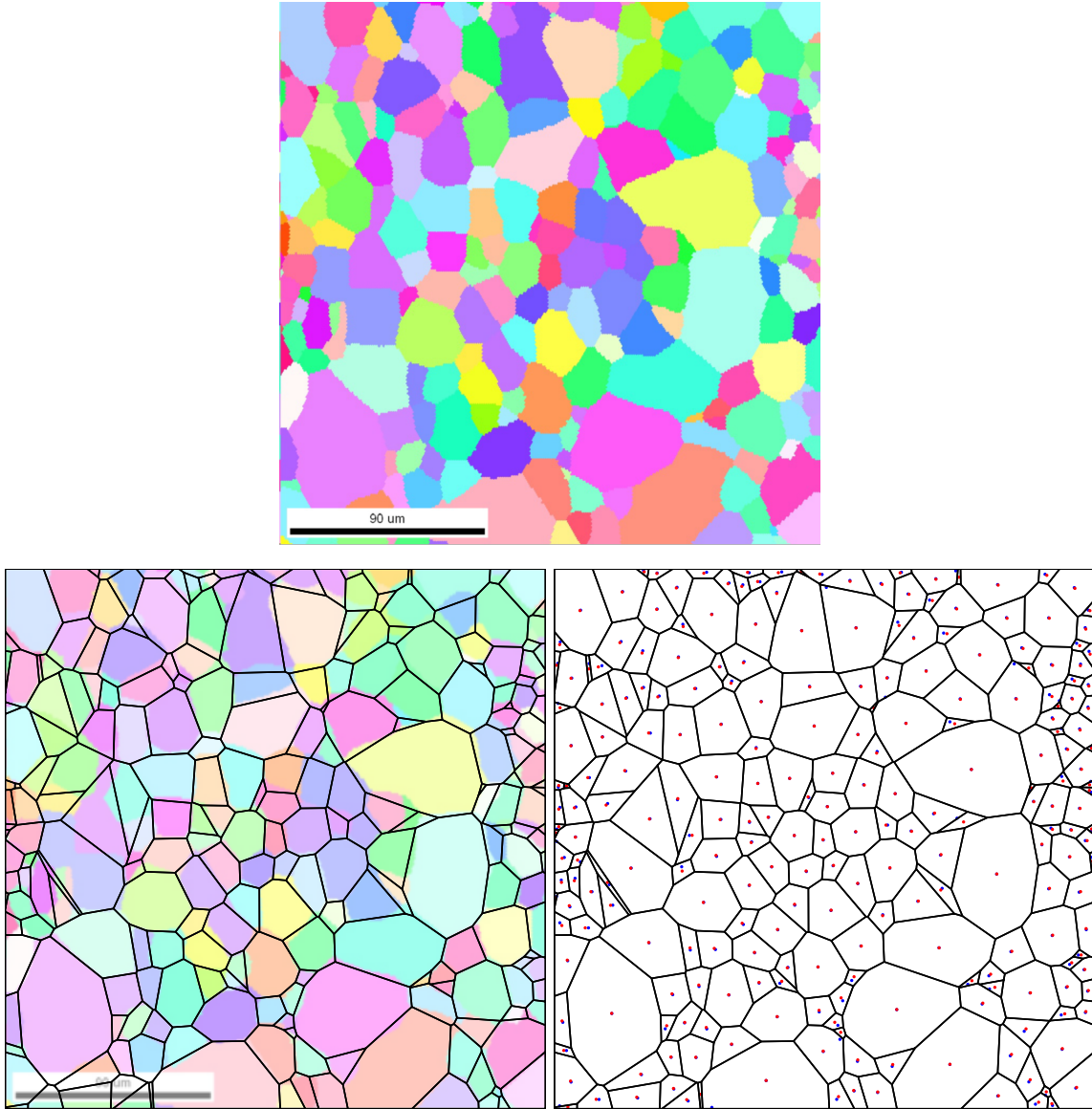


Figure 8: Fitting a Laguerre tessellation to an EBSD image; see Section 5.3. Top: The original EBSD image of a single-phase steel. The grains are coloured according to the orientation of the crystal lattice. We extracted the areas and centroids (\mathbf{v}, \mathbf{B}) of the grains from this EBSD image and then fitted a Laguerre tessellation to the image by solving the optimisation problem (5.2). Bottom-left: The fitted Laguerre diagram overlaid on the EBSD image. Bottom-right: The centroids \mathbf{B} from the EBSD data in blue and the centroids of the fitted Laguerre cells in red.

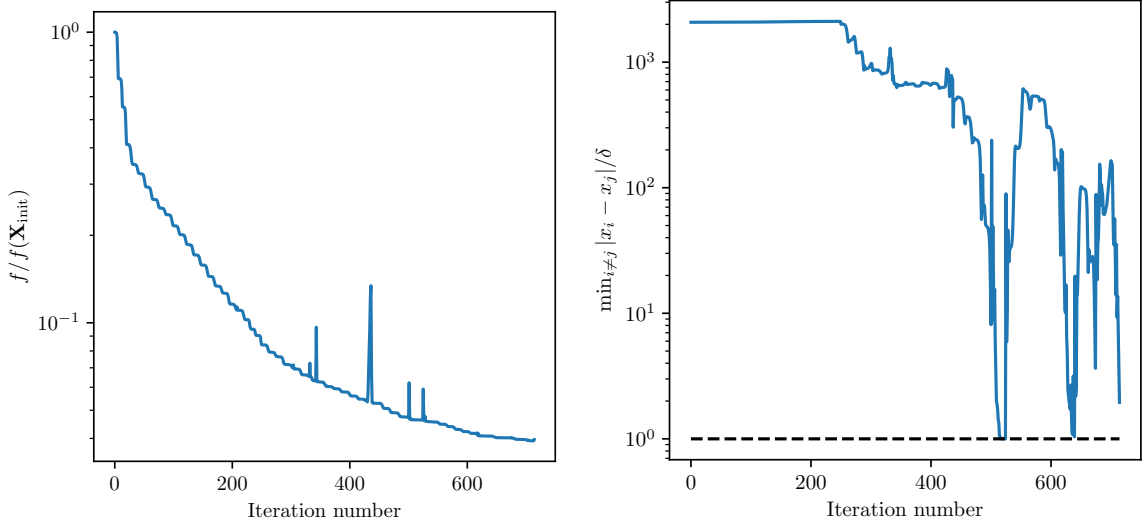


Figure 9: Fitting a Laguerre diagram to an EBSD image - convergence of the algorithm from Section 5.3. Left: Decay of the objective function f , normalised by its initial value $f(\mathbf{X}_{\text{init}})$. The algorithm terminated after 714 iterations and the objective function decreased by a factor of about 25. Right: The minimum distance between the seeds, normalised by the minimum allowed distance $\delta = 10^{-3}$. At least one of the constraints $c_{ij} \geq 0$ appears to be active for several iterations (the dotted line corresponds to an active constraint). This suggests that the seeds would collide in the absence of the constraints.

We briefly describe how Goal 1 can be addressed in the anisotropic setting, namely how to recover an anisotropic Laguerre tessellation given the volumes and centroids of its cells and the anisotropy matrices \mathbf{A} . We also state a uniqueness result.

Define the anisotropic optimal transport problem

$$\mathcal{T}_{\mathbf{A}}(\mathbf{X}, \mathbf{v}) = \inf_{T \in \mathcal{A}(\mathbf{X}, \mathbf{v})} \sum_{i=1}^n \int_{T^{-1}(\{x_i\})} |x - x_i|_{A_i}^2 dx, \quad (6.2)$$

where $\mathcal{A}(\mathbf{X}, \mathbf{v})$ is the set of admissible transport maps, which was defined in equation (2.7). As above, it is well-known that the optimal map $T^* : \Omega \rightarrow \{x_1, \dots, x_n\}$ partitions the domain Ω into anisotropic Laguerre cells, namely, there exists $\mathbf{w} = \mathbf{w}^*(\mathbf{X}; \mathbf{v}, \mathbf{A}) \in \mathbb{R}^n$ such that $(T^*)^{-1}(\{x_i\}) = \text{Lag}_i^{\mathbf{A}}(\mathbf{X}, \mathbf{w})$ for all i . The vector $\mathbf{w}^*(\mathbf{X}; \mathbf{v}, \mathbf{A})$ maximises the continuously differentiable, concave dual function $\mathcal{K}_{\mathbf{A}} : \mathbb{R}^n \rightarrow \mathbb{R}$,

$$\mathcal{K}_{\mathbf{A}}(\mathbf{w}) = \sum_{i=1}^n \int_{\text{Lag}_i^{\mathbf{A}}(\mathbf{X}, \mathbf{w})} (|x - x_i|_{A_i}^2 - w_i) dx + \sum_{i=1}^n w_i v_i,$$

which has gradient given by

$$\frac{\partial \mathcal{K}_{\mathbf{A}}}{\partial w_i}(\mathbf{w}) = v_i - \text{vol}(\text{Lag}_i^{\mathbf{A}}(\mathbf{X}, \mathbf{w})) \quad \forall i \in \{1, \dots, n\}.$$

In particular,

$$\text{vol}(\text{Lag}_i^{\mathbf{A}}(\mathbf{X}, \mathbf{w}^*(\mathbf{X}; \mathbf{v}, \mathbf{A}))) = v_i \quad \forall i \in \{1, \dots, n\}.$$

These results essentially follow from [38, Proposition 37, Theorem 40]. (A technical remark for experts in optimal transport theory: anisotropic Laguerre cells intersect in a set of Lebesgue-measure zero and hence the theory from [38] applies even though the anisotropic transport cost $c : \Omega \rightarrow \{x_1, \dots, x_n\}$ given by $c(x, x_i) = |x - x_i|_{A_i}^2$ does not satisfy the assumption of being *twisted* in general.) We define $L_i^{\mathbf{A}}(\mathbf{X}; \mathbf{v})$ to be the i^{th} anisotropic Laguerre cell in the tessellation with seeds \mathbf{X} , cell volumes \mathbf{v} and anisotropy matrices \mathbf{A} , and $c_i(\mathbf{X}; \mathbf{v}, \mathbf{A})$ to be its centroid:

$$L_i^{\mathbf{A}}(\mathbf{X}; \mathbf{v}) = \text{Lag}_i(\mathbf{X}, \mathbf{w}^*(\mathbf{X}; \mathbf{v}, \mathbf{A})), \quad c_i(\mathbf{X}; \mathbf{v}, \mathbf{A}) = \sigma(\text{Lag}_i(\mathbf{X}, \mathbf{w}^*(\mathbf{X}; \mathbf{v}, \mathbf{A}))).$$

The following theorem, which generalises Theorem 4.2 (iii),(iv), shows how an anisotropic Laguerre tessellation can be reconstructed from the volumes and centroids of its cells, given the anisotropy matrices A_i , by maximising a concave function.

Theorem 6.2 (Recovering an anisotropic Laguerre tessellation). *Given $(\mathbf{v}, \mathbf{B}) \in \mathcal{D}_n$ and a tuple of symmetric positive-definite matrices $\mathbf{A} = (A_1, \dots, A_n) \in (\mathbb{R}^{d \times d})^n$, define the function $H_{\mathbf{A}} : \mathbb{R}^{nd} \rightarrow \mathbb{R}$ by*

$$H_{\mathbf{A}}(\mathbf{X}) = H_{\mathbf{A}}(\mathbf{X}; (\mathbf{v}, \mathbf{B})) = \frac{1}{2} \mathcal{T}_{\mathbf{A}}(\mathbf{X}, \mathbf{v}) - \frac{1}{2} \sum_{i=1}^n v_i |x_i|_{A_i}^2 + \sum_{i=1}^n v_i x_i \cdot (A_i b_i). \quad (6.3)$$

If $\mathbf{X} \in \mathbb{D}_n$, then

$$H_{\mathbf{A}}(\mathbf{X}) = \frac{1}{2} \sum_{i=1}^n \int_{L_i^{\mathbf{A}}(\mathbf{X}; \mathbf{v})} |x - x_i|_{A_i}^2 dx - \frac{1}{2} \sum_{i=1}^n v_i |x_i|_{A_i}^2 + \sum_{i=1}^n v_i x_i \cdot (A_i b_i).$$

Then $H_{\mathbf{A}}$ is concave, continuously differentiable on the set of distinct seeds, $H_{\mathbf{A}} \in C^1(\mathbb{D}_n)$, and for all $\mathbf{X} \in \mathbb{D}_n$ the gradient of $H_{\mathbf{A}}$ is given by

$$\frac{\partial H_{\mathbf{A}}}{\partial x_i}(\mathbf{X}) = v_i A_i (b_i - c_i(\mathbf{X}; \mathbf{v}, \mathbf{A})) \quad \forall i \in \{1, \dots, n\}. \quad (6.4)$$

In particular, $\nabla H_{\mathbf{A}}(\mathbf{X}) = 0$ if and only if \mathbf{X} generates an anisotropic Laguerre tessellation with anisotropy matrices A_i and cells of volume v_i and centroids b_i .

Note that $H_{\mathbf{A}}$ does not contain the constant term $-\frac{1}{2} \int_{\Omega} |x|^2 dx$ that is present in the definition of H (compare equations (4.1) and (6.3)). This is because

$$\sum_{i=1}^n \int_{L_i^{\mathbf{A}}(\mathbf{X}; \mathbf{v})} |x|_{A_i}^2 dx \neq \int_{\Omega} |x|^2 dx$$

in general (unless $A_i = I_d$ for all i). Consequently the analogue of Theorem 4.2 (i) does not hold, namely, the maximum value of $H_{\mathbf{A}}$ is not zero if the data \mathbf{v} and \mathbf{B} are the volumes and centroids of an anisotropic Laguerre tessellation.

Sketch proof of Theorem 6.2. We just sketch the proof for brevity and because it is similar to the proof of Theorem 4.2. The proof that $H_{\mathbf{A}}$ is concave is exactly the same as the proof of

Theorem 4.2 (iii). We derive the gradient of $H_{\mathbf{A}}$ as follows. Let $\mathbf{X} \in \mathbb{D}_n$ and $\mathbf{Y} \in \mathbb{R}^{nd}$. Then

$$\begin{aligned}
H_{\mathbf{A}}(\mathbf{Y}) &\geq \frac{1}{2} \sum_{i=1}^n \int_{L_i^{\mathbf{A}}(\mathbf{X}; \mathbf{v})} |x - y_i|_{A_i}^2 dx - \frac{1}{2} \sum_{i=1}^n v_i |y_i|_{A_i}^2 + \sum_{i=1}^n v_i y_i \cdot (A_i b_i) \\
&= \frac{1}{2} \sum_{i=1}^n \int_{L_i^{\mathbf{A}}(\mathbf{X}; \mathbf{v})} |x - x_i|_{A_i}^2 dx - \frac{1}{2} \sum_{i=1}^n v_i |x_i|_{A_i}^2 + \sum_{i=1}^n v_i x_i \cdot (A_i b_i) \\
&\quad + \sum_{i=1}^n v_i (y_i - x_i) \cdot (A_i b_i) + \sum_{i=1}^n \int_{L_i^{\mathbf{A}}(\mathbf{X}; \mathbf{v})} (x_i - y_i) \cdot (A_i x) dx \\
&= H_{\mathbf{A}}(\mathbf{X}) + \sum_{i=1}^n (y_i - x_i) \cdot v_i A_i (b_i - c_i(\mathbf{X}; \mathbf{v}, \mathbf{A})).
\end{aligned}$$

In particular, the superdifferential of the concave function $H_{\mathbf{A}}$ at \mathbf{X} contains the point $(v_i A_i (b_i - c_i(\mathbf{X}; \mathbf{v}, \mathbf{A})))_{i=1}^n$. Similarly to the proof of [38, Theorem 40], it can be shown that this is the only point in the superdifferential and that it depends continuously on \mathbf{X} . Therefore $H_{\mathbf{A}}$ is continuously differentiable on \mathbb{D}_n with gradient given by (6.4), as required.

Alternatively, the gradient of $H_{\mathbf{A}}$ can be derived as follows. Let $\mathbf{X} \in \mathbb{D}_n$. By using the Kantorovich Duality Theorem from optimal transport theory, we can write

$$\begin{aligned}
H_{\mathbf{A}}(\mathbf{X}) &= \max_{\mathbf{w} \in \mathbb{R}^n} \left(\frac{1}{2} \int_{\Omega} \min_i (|x - x_i|_{A_i}^2 - w_i) dx + \sum_{i=1}^n v_i w_i - \frac{1}{2} \sum_{i=1}^n v_i |x_i|_{A_i}^2 + \sum_{i=1}^n v_i x_i \cdot (A_i b_i) \right) \\
&=: \max_{\mathbf{w} \in \mathbb{R}^n} G_{\mathbf{A}}(\mathbf{X}, \mathbf{w}).
\end{aligned}$$

Then it can be shown that

$$\frac{\partial H_{\mathbf{A}}}{\partial x_i}(\mathbf{X}) = \frac{\partial G_{\mathbf{A}}}{\partial x_i}(\mathbf{X}, \mathbf{w}^*(\mathbf{X}; \mathbf{v}, \mathbf{A})), \quad (6.5)$$

where $\mathbf{w}^*(\mathbf{X}; \mathbf{v}, \mathbf{A}) \in \mathbb{R}^n$ is any maximiser of $G_{\mathbf{A}}(\mathbf{X}, \cdot)$. Differentiating $G_{\mathbf{A}}$ gives

$$\begin{aligned}
\frac{\partial G_{\mathbf{A}}}{\partial x_i}(\mathbf{X}, \mathbf{w}) &= \frac{1}{2} \int_{\Omega} \frac{\partial}{\partial x_i} \min_k (|x - x_k|_{A_k}^2 - w_k) dx - v_i A_i x_i + v_i A_i b_i \\
&= \frac{1}{2} \sum_{k=1}^n \int_{L_{\text{Lag}_k^{\mathbf{A}}}(\mathbf{X}, \mathbf{w})} \frac{\partial}{\partial x_i} (|x - x_k|_{A_k}^2 - w_k) dx - v_i A_i x_i + v_i A_i b_i \quad (6.6)
\end{aligned}$$

$$= \int_{L_{\text{Lag}_i^{\mathbf{A}}}(\mathbf{X}, \mathbf{w})} A_i (x_i - x) dx - \sum_{i=1}^n v_i A_i x_i + \sum_{i=1}^n v_i A_i b_i \quad (6.7)$$

for any $\mathbf{w} \in \mathbb{R}^n$. Combining (6.5) and (6.7) gives the gradient of $H_{\mathbf{A}}$, as claimed. \square

The following result generalises Theorem 4.5.

Theorem 6.3 (Uniqueness of anisotropic compatible diagrams). *Let $(\mathbf{v}, \mathbf{B}) \in \mathcal{D}_n$ and let $\mathbf{A} = (A_1, \dots, A_n) \in (\mathbb{R}^{d \times d})^n$ be a tuple of symmetric positive-definite matrices. Suppose $\mathbf{X}, \mathbf{Y} \in \mathbb{D}_n$ are such that $\{L_i^{\mathbf{A}}(\mathbf{X}; \mathbf{v})\}_{i=1}^n$ and $\{L_i^{\mathbf{A}}(\mathbf{Y}; \mathbf{v})\}_{i=1}^n$ are compatible with the data (\mathbf{v}, \mathbf{B}) in the sense that*

$$c_i(\mathbf{X}; \mathbf{v}, \mathbf{A}) = c_i(\mathbf{Y}; \mathbf{v}, \mathbf{A}) = b_i \quad \forall i \in \{1, \dots, n\}.$$

Then

$$L_i^{\mathbf{A}}(\mathbf{X}; \mathbf{v}) = L_i^{\mathbf{A}}(\mathbf{Y}; \mathbf{v}) \quad \forall i \in \{1, \dots, n\}.$$

In other words, an anisotropic Laguerre tessellation is uniquely determined by the volumes and centroids of its cells and its anisotropy matrices.

Proof. The proof is almost identical to the proof of Theorem 4.5 and so we do not repeat it here. It is simply a matter of replacing Euclidean norms with anisotropic norms. \square

7 Conclusions and future directions

In this paper we have given a complete theoretical answer to Goal 1; we proved that a Laguerre tessellation is uniquely determined by the volumes and centroids of its cells and that it can be recovered using convex optimisation (Theorems 4.5 and 4.6). We performed some preliminary numerical experiments in Section 5.1 but there is room for improvement here. Since we used a gradient-based method to maximise H , and ∇H is only defined where the seeds are distinct, we introduced the extra constraints $c_{ij} \geq 0$, which destroyed the convexity of the constraint set. In future work it would be interesting to use non-smooth convex optimisation (such as a proximal method) to maximise H on the ball and preserve the convexity of the problem.

Goal 2 turned out to be more challenging and, for some data (\mathbf{v}, \mathbf{B}) , even to be ill-posed. We start with the positive results. If the target data (\mathbf{v}, \mathbf{B}) satisfies the implicit assumption that the maximiser of H on a ball is achieved at a point with distinct seeds (and under some other generic assumptions), then we found a complete theoretical answer to Goal 2; local minimisers of the fitting error f can be found by solving a convex optimisation problem (Theorem 4.11). As for Goal 1, our numerical simulations could be improved to exploit this convexity. Nevertheless, we still obtained good results for the materials science application in Section 5.3.

The implicit assumption on the target data (\mathbf{v}, \mathbf{B}) , however, is restrictive. In Section 5.2.2 we gave numerical evidence that there exists data (\mathbf{v}, \mathbf{B}) such that the maximiser of H on a ball is achieved at a point in the set $\mathbb{R}^{nd} \setminus \mathbb{D}_n$ of non-distinct seeds, where ∇H is not defined. In this case we believe that the infimum of $f = |\nabla H|^2$ is not attained. The non-existence of a minimiser of f on \mathbb{D}_n can also be checked analytically for a very simple example with two seeds. To obtain a well-posed optimisation problem for all data (\mathbf{v}, \mathbf{B}) , in Sections 5.2 and 5.3 we supplemented (NLS) with the constraints $c_{ij} \geq 0$. An alternative approach could be to use a different objective function entirely. For example, we could drop the constraint that the volumes of the cells are fitted exactly, and replace the centroid error $f(\mathbf{X})$ by a function of (\mathbf{X}, \mathbf{w}) measuring a weighted sum of the volume error and the centroid error.

It is an open problem to characterise the data (\mathbf{v}, \mathbf{B}) for which (NLS) attains its infimum. The simulations in Section 5.2.2 suggest that this set could be quite a small neighbourhood of the data (\mathbf{v}, \mathbf{B}) for which there exists a compatible diagram. It is also an open problem to find sufficient conditions on (\mathbf{v}, \mathbf{B}) for there to exist a compatible diagram; in Section 4.3 we only gave necessary conditions. We hope that this paper inspires further work on Goal 2.

Acknowledgements. The authors thank Piet Kok, Filippo Santambrogio, Karo Sedighiani and Wil Spanjer for fruitful discussions. The EBSD image in Figure 8 was provided by Tata Steel Europe. DPB acknowledges financial support from the EPSRC grant EP/V00204X/1

Mathematical Theory of Polycrystalline Materials. MP thanks the Centre for Doctoral Training in Mathematical Modelling, Analysis and Computation (MAC-MIGS), funded by EPSRC grant EP/S023291/1.

References

- [1] Geogram. <https://github.com/BrunoLevy/geogram>. Accessed: 2024-05-06.
- [2] MATLAB-SDOT. <https://github.com/DPBourne/MATLAB-SDOT>. Accessed: 2024-05-06.
- [3] pysdot. <https://github.com/sd-ot/pysdot>. Accessed: 2024-05-06.
- [4] A. Alpers, A. Brieden, P. Gritzmann, A. Lyckegaard, and H. F. Poulsen. Generalized balanced power diagrams for 3d representations of polycrystals. *Philosophical Magazine*, 95(9):1016–1028, 2015.
- [5] A. Alpers, M. Fiedler, P. Gritzmann, and F. Klemm. Dynamic grain models via fast heuristics for diagram representations. *Philosophical Magazine*, 103(10):948–968, 2023.
- [6] A. Alpers, M. Fiedler, P. Gritzmann, and F. Klemm. Turning grain maps into diagrams. *SIAM Journal on Imaging Sciences*, 16(1):223–249, 2023.
- [7] H. Altendorf, F. Latourte, D. Jeulin, M. Faessel, and L. Saintoyant. 3d reconstruction of a multiscale microstructure by anisotropic tessellation models. *Image Analysis and Stereology*, 33(2):121–130, 2014.
- [8] F. Aurenhammer. A criterion for the affine equivalence of cell complexes in \mathbb{R}^d and convex polyhedra in \mathbb{R}^{d+1} . *Discrete & Computational Geometry*, 2:49–64, 1987.
- [9] F. Aurenhammer, F. Hoffmann, and B. Aronov. Minkowski-type theorems and least-squares clustering. *Algorithmica*, 20:61–76, 1998.
- [10] F. Aurenhammer, R. Klein, and Lee D.-T. *Voronoi Diagrams and Delaunay Triangulations*. World Scientific, 2013.
- [11] E. Birgin, A. Laurain, and T. Menezes. Sensitivity analysis and tailored design of minimization diagrams. *Mathematics of Computation*, 92(344):2715–2768, 2023.
- [12] P. V. M. Blagojević and G. M. Ziegler. Convex equipartitions via equivariant obstruction theory. *Israel Journal of Mathematics*, 200:49–77, 2014.
- [13] M. Bock, A. K. Tyagi, J.-U. Kreft, and W. Alt. Generalized Voronoi tessellation as a model of two-dimensional cell tissue dynamics. *Bulletin of Mathematical Biology*, 72:1696–1731, 2010.
- [14] J.-D. Boissonnat, C. Wormser, and M. Yvinec. Curved Voronoi diagrams. In *Effective Computational Geometry for Curves and Surfaces*, pages 67–116. Springer, 2006.
- [15] D. P. Bourne, P. J. J. Kok, S. . Roper, and W. D. T. Spanjer. Laguerre tessellations and polycrystalline microstructures: a fast algorithm for generating grains of given volumes. *Philosophical Magazine*, 100(21):2677–2707, 2020.

- [16] D. P. Bourne, M Pearce, and S. M. Roper. Geometric modelling of polycrystalline materials: Laguerre tessellations and periodic semi-discrete optimal transport. *Mechanics Research Communications*, 127:104023, 2023.
- [17] D. P. Bourne and S. M. Roper. Centroidal power diagrams, Lloyd’s algorithm, and applications to optimal location problems. *SIAM Journal on Numerical Analysis*, 53(6):2545–2569, 2015.
- [18] O. Busaryev, T. K. Dey, H. Wang, and Z. Ren. Animating bubble interactions in a liquid foam. *ACM Transactions on Graphics*, 31(4), 2012.
- [19] M. Buze, J. Feydy, S. M. Roper, K. Sedighiani, and D. P. Bourne. Anisotropic power diagrams for polycrystal modelling: Efficient generation of curved grains via optimal transport. *arXiv:2403.03571*, 2024.
- [20] F. de Gournay, J. Kahn, and L. Lebrat. Differentiation and regularity of semi-discrete optimal transport with respect to the parameters of the discrete measure. *Numerische Mathematik*, 141(2):429–453, 2018.
- [21] D. Depriester and R. Kubler. Radical Voronoi tessellation from random pack of polydisperse spheres: Prediction of the cells’ size distribution. *Computer-Aided Design*, 107:37–49, 2019.
- [22] A. Diez and J. Feydy. An optimal transport model for dynamical shapes, collective motion and cellular aggregates. *arXiv:2402.17086*, 2024.
- [23] Q. Duan, D. Kroese, T. Brereton, A. Spettl, and V. Schmidt. Inverting Laguerre tessellations. *The Computer Journal*, 57:1431–1440, 2014.
- [24] Z. Fan, Y. Wu, X. Zhao, and Y. Lu. Simulation of polycrystalline structure with Voronoi diagram in Laguerre geometry based on random closed packing of spheres. *Computational Materials Science*, 29(3):301–308, 2004.
- [25] T. O. Gallouët, Q. Mérigot, and A. Natale. Convergence of a Lagrangian discretization for barotropic fluids and porous media flow. *SIAM Journal on Mathematical Analysis*, 54(3):2990–3018, 2022.
- [26] P. M. Gruber. *Convex and Discrete Geometry*. Springer, 2007.
- [27] C. Jung and C. Redenbach. An analytical representation of the 2d generalized balanced power diagram. *Computational Geometry*, 121:102101, 2024.
- [28] J. Kitagawa, Q. Mérigot, and B. Thibert. Convergence of a newton algorithm for semi-discrete optimal transport. *Journal of the European Mathematical Society*, 21(9):2603–2651, 2019.
- [29] J. Kuhn, M. Schneider, P. Sonnweber-Ribic, and T. Böhlke. Fast methods for computing centroidal Laguerre tessellations for prescribed volume fractions with applications to microstructure generation of polycrystalline materials. *Computer Methods in Applied Mechanics and Engineering*, 369:113175, 2020.

- [30] M. Kühn and M. O. Steinhauser. Modeling and simulation of microstructures using power diagrams: Proof of the concept. *Applied Physics Letters*, 93(3):034102, 2008.
- [31] C. Lautensack and S. Zuyev. Random Laguerre tessellations. *Advances in Applied Probability*, 40(3):630–650, 2008.
- [32] B. Lévy. A numerical algorithm for L2 semi-discrete optimal transport in 3D. *ESAIM: Mathematical Modelling and Numerical Analysis*, 49(6):1693–1715, 2015.
- [33] B. Lévy. Partial optimal transport for a constant-volume Lagrangian mesh with free boundaries. *Journal of Computational Physics*, 451:110838, 2022.
- [34] A. Liebscher. Laguerre approximation of random foams. *Philosophical Magazine*, 95(25):2777–2792, 2015.
- [35] A. Lyckegaard, E. M. Lauridsen, W. Ludwig, R. W. Fonda, and H. F. Poulsen. On the use of Laguerre tessellations for representations of 3d grain structures. *Advanced Engineering Materials*, 13(3):165–170, 2011.
- [36] Q. Mérigot and J.-M. Mirebeau. Minimal geodesics along volume-preserving maps, through semidiscrete optimal transport. *SIAM Journal on Numerical Analysis*, 54(6):3465–3492, 2015.
- [37] Q. Mérigot, F. Santambrogio, and C. Sarrazin. Non-asymptotic convergence bounds for Wasserstein approximation using point clouds. In M. Ranzato, A. Beygelzimer, Y. Dauphin, P.S. Liang, and J. Wortman Vaughan, editors, *Proceedings of Advances in Neural Information Processing Systems 34 (NeurIPS 2021)*. 2021.
- [38] Q. Mérigot and B. Thibert. Optimal transport: discretization and algorithms. In A. Bonito and R. H. Nochetto, editors, *Geometric Partial Differential Equations - Part II*, volume 22 of *Handbook of Numerical Analysis*, pages 133–212. North-Holland, 2021.
- [39] J. Meyron. Initialization procedures for discrete and semi-discrete optimal transport. *Computer-Aided Design*, 115:13–22, 2019.
- [40] J. Meyron, Q. Mérigot, and B. Thibert. Light in power: a general and parameter-free algorithm for caustic design. *ACM Transactions on Graphics*, 37(6):1–13, 2018.
- [41] J. Nocedal and S. J. Wright. *Numerical Optimization*. Springer, 2nd edition, 2006.
- [42] A. Okabe, B. Boots, K. Sugihara, and S. N. Chiu. *Spatial Tessellations. Concepts and Applications of Voronoi Diagrams*. Wiley, 2nd edition, 2000.
- [43] L. Petrich, O. Furat, M. Wang, C. E. Krill III, and V. Schmidt. Efficient fitting of 3D tessellations to curved polycrystalline grain boundaries. *Frontiers in Materials*, 8:760602, 2021.
- [44] L. Petrich, J. Staněk, M. Wang, D. Westhoff, L. Heller, P. Šittner, C. E. Krill III, V. Beneš, and V. Schmidt. Reconstruction of grains in polycrystalline materials from incomplete data using Laguerre tessellations. *Microscopy and Microanalysis*, 25(3):743–752, 2019.

- [45] R. Quey and L. Renversade. Optimal polyhedral description of 3D polycrystals: Method and application to statistical and synchrotron X-ray diffraction data. *Computer Methods in Applied Mechanics and Engineering*, 330:308–333, 2018.
- [46] R. T. Rockafellar. *Convex Analysis*. Princeton, 1970.
- [47] F. Santambrogio. *Optimal Transport for Applied Mathematicians*. Birkhäuser, 2015.
- [48] O. Šedivý, T. Brereton, D. Westhoff, L. Polívka, V. Beneš, V. Schmidt, and A. Jäger. 3D reconstruction of grains in polycrystalline materials using a tessellation model with curved grain boundaries. *Philosophical Magazine*, 96(18):1926–1949, 2016.
- [49] A. Spettl, T. Brereton, Q. Duan, T. Werz, C. E. Krill III, D. P. Kroese, and V. Schmidt. Fitting Laguerre tessellation approximations to tomographic image data. *Philosophical Magazine*, 96(2):166–189, 2016.
- [50] K. Teferra and D. J. Rowenhorst. Direct parameter estimation for generalised balanced power diagrams. *Philosophical Magazine Letters*, 98(2):79–87, 2018.
- [51] Y. Wu, W. Zhou, B. Wang, and F. Yang. Modeling and characterization of two-phase composites by Voronoi diagram in the Laguerre geometry based on random close packing of spheres. *Computational Materials Science*, 47(4):951–961, 2010.
- [52] S.-Q. Xin, B. Lévy, Z. Chen, L. Chu, Y. Yu, C. Tu, and W. Wang. Centroidal power diagrams with capacity constraints: Computation, applications, and extension. *ACM Transactions on Graphics*, 35(6):244:1–244:12, 2016.